Volume 4 | Issue 2 | August 2025

EISSN 2822-2318

Official Journal of Turkish Society of Magnetic Resonance

CRMRI

Current Research in MRI

AVES

curremr.com

TMRD
TÜRK MANYETİK REZONANS DERNEĞİ
TURKISH SOCIETY OF MAGNETIC RESONANCE

Current Research in MRI

TMRD
TÜRK MANYETİK REZONANS DERNEĞİ
TURKISH SOCIETY OF MAGNETIC RESONANCE

AVES

General Manager
İbrahim KARA

Publications Director
Deniz KAYA

Finance Coordinator
Gözde DOĞAN

Publications Coordinators
Nisanur ATICI
Şeref Mert GÜCÜN
Lütfiye ÇETİN
Şevval AKKAYA

Web Coordinator
Ayça Nur SEZEN

Contact
Address: Halaskargazi Mah. Halaskargazi Cad. No: 38-66E İç Kapı No: 215 Şişli, İstanbul, Türkiye.
Phone: +90 212 217 17 00
E-mail: info@avespublishing.com

Current Research in MRI

About the Current Research in MRI

Current Research in MRI is a peer reviewed, open access, online-only journal published by the Turkish Society of Magnetic Resonance.

Current Research in MRI is a triannual journal that is published in English in April, August, and December.

Indexing
Current Research in MRI is covered in the following indexing database;

- EBSCO
- DOAJ
- China National Knowledge Infrastructure (CNKI)

All content published in the journal is permanently archived in Portico.

Aims, Scope, and Audience

Current Research in MRI aims to publish studies of the highest scientific and clinical value. It also encourages the submission of high-quality research in the field of radiology.

Current Research in MRI covers a wide range of topics related to radiology.

Current Research in MRI publishes original articles, reviews, case reports, and letters to the editor that are prepared in accordance with ethical guidelines.

The target audience of the journal includes healthcare professionals, physicians, and researchers who are interested in or working in the field of radiology.

You can reach the current version of the instructions to authors at https://curremr.com/EN

Editor in Chief: Mecit Kantarcı
Address: Department of Radiology, Erzincan Binali Yıldırım University School of Medicine, Erzincan, Türkiye
E-mail: akkanrad@hotmail.com

Publisher: Turkish Society of Magnetic Resonance
Address: Konak Mah. 858. Sok. No: 2 Çakıroğlu İş Hanı Kat: 5 Daire: 55 Konak / İzmir, Türkiye

Publishing Services: AVES
Address: Halaskargazi Mah. Halaskargazi Cad. No: 38-66E İç Kapı No: 215 Şişli, İstanbul, Türkiye.
Phone: +90 212 217 17 00
E-mail: info@avespublishing.com
Webpage: www.avespublishing.com

Current Research in MRI

CONTENTS

ORIGINAL ARTICLES

Current Research in MRI

Original Article

Correlation of Contrast Enhancement Patterns with Molecular Subtypes in Dynamic Contrast-Enhanced Magnetic Resonance Imaging of Breast Malignancies

Ali Fuat Tekin[1], Yiğit Can Kartal[1], Volkan Taşçi[2], Serçin Özkök[1], İsmet Tolu[3]

[1]Department of Radiology, Başakşehir Çam and Sakura Hospital, İstanbul, Türkiye
[2]Department of Radiology, Sakarya Training and Research Hospital, İstanbul, Türkiye
[3]Department of Radiology, Karamanoğlu Mehmet Bey University Hospital, Sakarya, Türkiye

Cite this article as: Tekin AF, Kartal YC, Taşçi V, Özkök S, Tolu İ. Correlation of contrast enhancement patterns with molecular subtypes in dynamic contrast-enhanced magnetic resonance imaging of breast malignancies. *Current Research in MRI*, 2025;4(2):27-34.

Corresponding author: Ali Fuat Tekin, e-mail: aftrad333@gmail.com

Received: April 9, 2025 **Revision Requested:** April 22, 2025 **Last Revision Received:** July 8, 2025 **Accepted:** July 18, 2025 **Publication Date:** October 30, 2025

DOI: 10.5152/CurrResMRI.2025.25117

Abstract

Objective: This study aimed to evaluate the use of dynamic contrast-enhanced magnetic resonance imaging (DCE-MRI) to predict the molecular subtypes of breast cancer, with a focus on receptor status.

Methods: The authors retrospectively reviewed breast MRI scans of 154 patients with histopathologically confirmed invasive breast carcinoma who underwent preoperative DCE-MRI between January 2010 and January 2015. Tumors were classified as Luminal A, Luminal B, human epidermal growth factor receptor 2 (HER2)-enriched, or triple-negative based on IHC for ER, PR, and HER2. Contrast-enhanced magnetic resonance imaging findings included time–signal intensity curve patterns and enhancement characteristics. The axillary nodal status and background parenchymal enhancement (BPE) were also recorded.

Results: In total, 154 patients (mean age: 51.4 years; range, 24-80 years) were evaluated. Magnetic resonance imaging findings demonstrated homogeneous internal contrast in 31%, heterogeneous contrast in 40%, and rim enhancement in 29% of the tumors. Regarding molecular markers, ER positivity was observed in 39.4% of patients, PR positivity in 43.5%, and HER2 positivity in 36.4%. The tumor subtype distribution included Luminal A (17.4%), Luminal B (36.8%), and triple-negative (44.5%). Type 1 enhancement was observed in 37.7% of patients, type 2 in 36.4%, and type 3 in 26.0%. A significant relationship was identified between Luminal A subtype and type 3 contrast enhancement ($P < .05$). Luminal B subtype was significantly associated with increased BPE (types 1 and 2) and contralateral breast enhancement ($P < .05$). No significant associations were observed between molecular markers or subtypes and lymph node positivity.

Conclusion: Human epidermal growth factor receptor 2-positive tumors have a plateau perfusion pattern and washout kinetics, and triple-negative tumors often exhibit rapid washout. These findings support the continued investigation of DCE-MRI for early subtype prediction and personalized treatment planning.

Keywords Breast cancer, contrast-enhanced magnetic resonance imaging, imaging, magnetic resonance imaging, molecular subtypes

INTRODUCTION

Breast cancer remains a leading cause of cancer-related mortality among women worldwide, and its clinical and biological heterogeneity necessitates precise molecular subtyping to guide personalized treatment strategies.[1] Breast cancer is classified into Luminal A, Luminal B, human epidermal growth factor receptor 2 (HER2)-enriched, and triple-negative subtypes, based on estrogen receptor (ER), progesterone receptor (PR), and HER2 status, and has revolutionized therapeutic decision-making and prognostication.[1] Although immunohistochemistry (IHC) and genomic profiling are the current standards for subtyping, these methods are invasive and time-consuming, highlighting the need for noninvasive predictive tools.[2]

Dynamic contrast-enhanced magnetic resonance imaging (DCE-MRI) has emerged as a pivotal modality for breast cancer diagnosis, offering high sensitivity for lesion detection and characterization through perfusion and kinetic analyses.[3] Contrast-enhanced magnetic resonance imaging parameters, such as time–signal intensity curves (TIC) and enhancement patterns, reflect tumor angiogenesis and vascular permeability, which are influenced by molecular pathways.[4] Previous studies have explored the associations between MRI features and receptor status; for instance, HER2-positive and triple-negative tumors often exhibit rapid washout kinetics, while luminal subtypes may demonstrate persistent or plateau enhancement.[5,6] However, inconsistencies persist regarding specific correlations, particularly for Luminal A/B differentiation and background parenchymal enhancement (BPE) implications.[7,8]

Recent radiogenomic investigations suggest that DCE-MRI phenotypes may mirror the underlying genetic expression, with rim enhancement linked to high-grade tumors and heterogeneous internal enhancement associated with proliferative markers.[9,10] Despite these advances, comprehensive

analyses correlating TIC patterns, BPE, and axillary nodal status across all the molecular subtypes remain limited. This gap impedes the integration of MRI biomarkers into clinical subtype algorithms.

This study evaluated the potential of DCE-MRI to predict molecular subtypes of invasive breast carcinoma, focusing on enhancement kinetics, BPE, and nodal involvement. By elucidating subtype-specific imaging signatures, the authors aim to advance noninvasive stratification, potentially reducing the dependency on biopsy for treatment planning.

MATERIAL AND METHODS

Patient Selection and Inclusion Criteria

Ethical approval for the study was obtained from the Konya Necmettin Erbakan University institutional review board (Approval No. 2214/5, dated 20.01.2016). This retrospective study included 154 female patients (age range: 24-80 years; mean age: 52 years) who underwent preoperative DCE-MRI between January 2010 and January 2015. All patients had histopathologically confirmed invasive breast cancer based on core needle biopsy and subsequent surgical specimen analysis. Demographic data and pathological findings were collected from the hospital information system. Patients who had received neoadjuvant therapy before MRI or had premalignant breast cancer were excluded. Contrast-enhanced magnetic resonance imaging examinations that were unavailable for review and cases without definitive pathology results for ER, PR, and HER2 status were also excluded. Given the retrospective design of the study, the requirement for informed consent was waived by the ethics committee.

Magnetic Resonance Imaging Acquisition Protocol and Image Analysis

All breast MRI examinations were performed using a 1.5 Tesla scanner (Siemens Magnetom Avanto, Erlangen, Germany) with a dedicated 16-channel bilateral breast coil. Patients were imaged in the prone position. The MRI protocol included high-resolution morphological sequences, followed by dynamic contrast-enhanced imaging, as presented below.

Precontrast Sequences: Axial and sagittal localizer images were obtained, followed by T1-weighted spin-echo sequences without fat suppression in the coronal plane (TR, 313 ms; TE: 4.5 ms, slice thickness, 3 mm) and T2-weighted fast spin-echo sequences in the axial plane (TR: 9710 ms, TE: 190 ms, slice thickness 3 mm). An axial STIR sequence (Turbo Inversion Recovery Magnitude, TRIM) was also acquired for additional lesion characterization.

Dynamic Contrast-Enhanced Sequence: A 3D T1-weighted gradient-echo sequence (TR: 4.4 ms, TE: 1.3 ms, flip angle as per protocol, slice thickness: 1 mm) was performed in the axial plane. First, a baseline (precontrast) image was acquired. A standard dose of gadolinium contrast (0.1 mmol/kg gadopentetate dimeglumine) was injected intravenously at 2 mL/s, followed by a saline flush. Serial post-contrast images were obtained immediately after injection, with at least 3-5 sequential acquisitions covering up to 7-8 minutes. All post-contrast images were automatically subtracted from the precontrast image using MRI system software to highlight contrast uptake and produce multiple time points for dynamic analysis.

Image Analysis: All MR images were reviewed on a workstation by a radiologist with at least 10 years of experience in breast imaging. The lesions were identified and characterized according to the BI-RADS MRI lexicon.[9] For each lesion, morphology and enhancement features were recorded.

1-The lesion shape was categorized (e.g., round, oval, lobulated, irregular stellate, or linear forms).

2-The lesion margin was defined as well-defined or poorly defined/spiculated.

The internal enhancement pattern of each mass on post-contrast images was classified as homogeneous (uniform enhancement), heterogeneous (mixed enhancement), or rim enhancement (peripheral enhancement with a central low signal), according to standard BI-RADS descriptors. These 3 contrast enhancement patterns were used to describe the spatial distribution of the contrast within the tumor.

Time–signal intensity curves to evaluate kinetic characteristics for each lesion were generated using a dedicated software platform (Siemens Syngo.via, Siemens Healthineers). A region of interest (ROI) with standardized dimensions (approximately 5-10 mm^2, adjusted based on lesion size and image resolution) was manually placed on the area of the tumor demonstrating the strongest early enhancement, carefully avoiding necrotic, cystic, or nonenhancing regions. In patients with multiple lesions, the largest or most clinically significant lesion was used for kinetic analysis. Signal intensities within the ROI were recorded across sequential dynamic contrast-enhanced phases to plot the enhancement curve. The kinetic curves of each lesion were then categorized into 1 of the 3 standard kinetic patterns based on their shape:[9]

Type 1 (Persistent): Signal intensity continuously increases over time (progressive enhancement with no plateau or washout) (Figure 1).

Type 2 (Plateau): Signal intensity rises initially and then levels off (plateaus) in later phases (suggesting intermediate kinetics) (Figure 2).

Type 3 (Washout): Signal intensity increases rapidly and then decreases in the late phase (initial enhancement followed by washout, often indicating more aggressive behavior) (Figure 3).

In addition to lesion analysis, BPE was also evaluated. Two ROIs of similar size were placed in visually normal fibroglandular tissue: 1 in the ipsilateral breast (outside the tumor area) and 1 in the corresponding location of the contralateral breast. Time–signal intensity curves

MAIN POINTS

- Luminal A breast tumors show a significant association with washout-type contrast enhancement kinetics on dynamic DCE-MRI.
- Luminal B tumors frequently exhibit moderate-to-marked BPE and contralateral breast enhancement, reflecting their aggressive biological characteristics.
- Human epidermal growth factor receptor 2-positive and triple-negative breast cancers predominantly demonstrate rapid washout kinetics, though HER2-positive tumors may also exhibit plateau-type enhancement, highlighting molecular complexity.
- Contrast-enhanced magnetic resonance imaging features alone are not reliable predictors for axillary lymph node involvement across breast cancer molecular subtypes.
- Contrast-enhancement kinetics on DCE-MRI could support non-invasive molecular subtyping, potentially reducing reliance on invasive biopsy procedures for personalized treatment decisions.

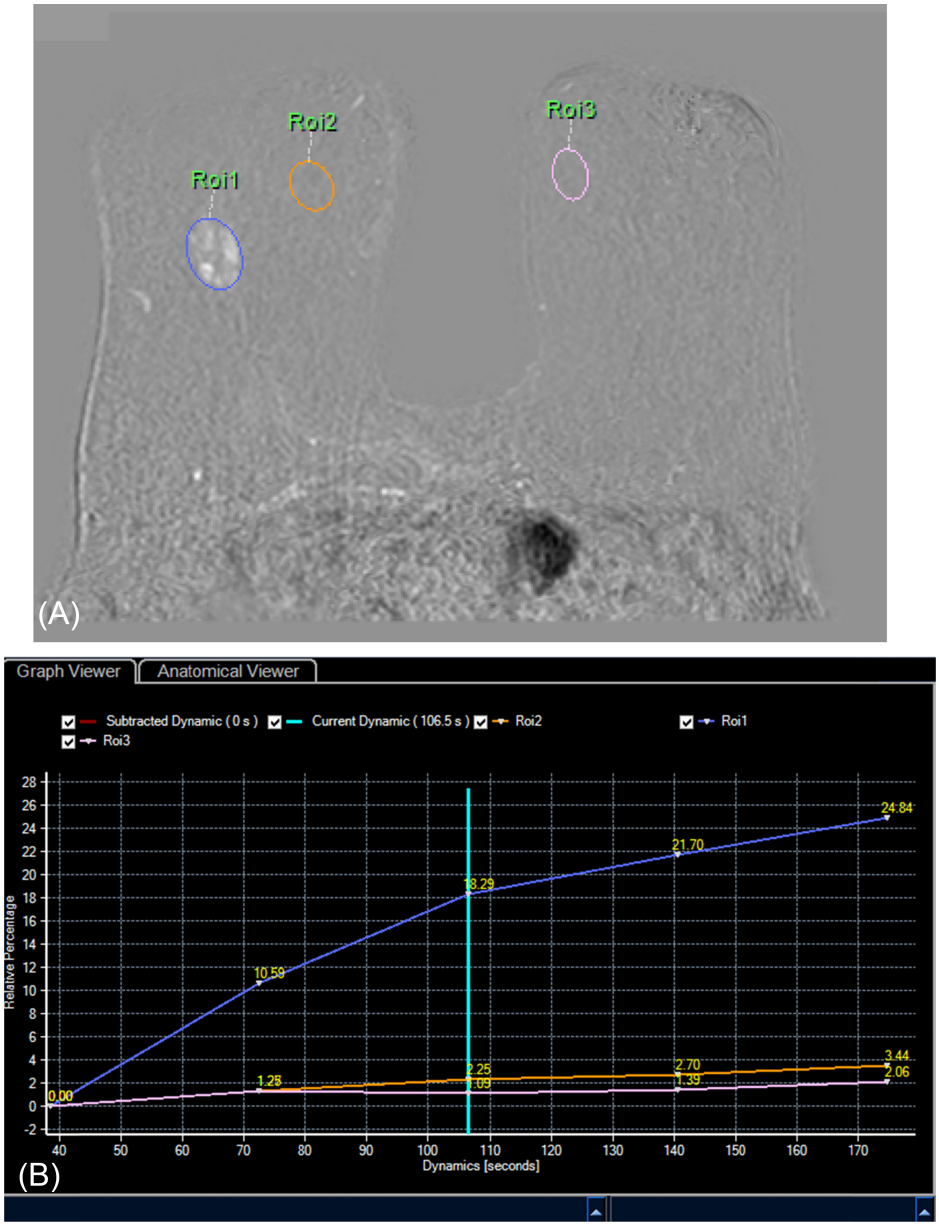

Figure 1 A 70-year-old patient is presented with an oval shaped and spiculated margin mass measuring 9 × 8 mm on the right breast at 11 o'clock, which is followingly diagnosed as invasive ductal carcinoma. Histopathological examination reveals estrogen receptor (−), progesterone receptor (+), and c-erbB2 (−). A) The mean curve measurement of mass enhancement, non-mass enhancement, and parenchymal enhancement in the contralateral breast on dynamic contrast-enhanced breast MRI using ROI, (B) the time–intensity curve displays type 1 pattern of mass enhancement, non-mass enhancement, and the parenchymal enhancement of the contralateral breast.

were also generated for these ROI locations to evaluate parenchymal enhancement characteristics.

Histopathological Assessment and Receptor Status Classification

All patients underwent breast surgery (mastectomy or lumpectomy with axillary evaluation) after the breast MRI. The tumor type and grade were recorded.

Estrogen receptor and progesterone receptor status was determined by IHC staining for estrogen and PRs in the tumor tissue. The percentage of cells with strong, moderate, or weak nuclear staining was assessed and weighted; tumors with an IHC score above a defined cutoff (corresponding roughly to >1% of nuclei positive) were considered ER- or PR-positive. Tumors with essentially no nuclear staining or only minimal staining (<1% or below the cut-off score) were considered negative for ER or PR. HER2 status was evaluated by IHC for the HER2/neu (c-erbB2) protein. Staining was scored on a 0-3+ scale, following the ASCO/CAP guidelines.[10] For each case, the ER, PR, and HER2 statuses were recorded as positive or negative. Tumors were categorized into molecular subtypes for further analysis as (1) Luminal A, 2) Luminal B, (3) HER2-enriched, and (4) triple negative.[10]

Axillary lymph node dissection or sentinel node biopsy was performed in all cases, and lymph node involvement (presence of

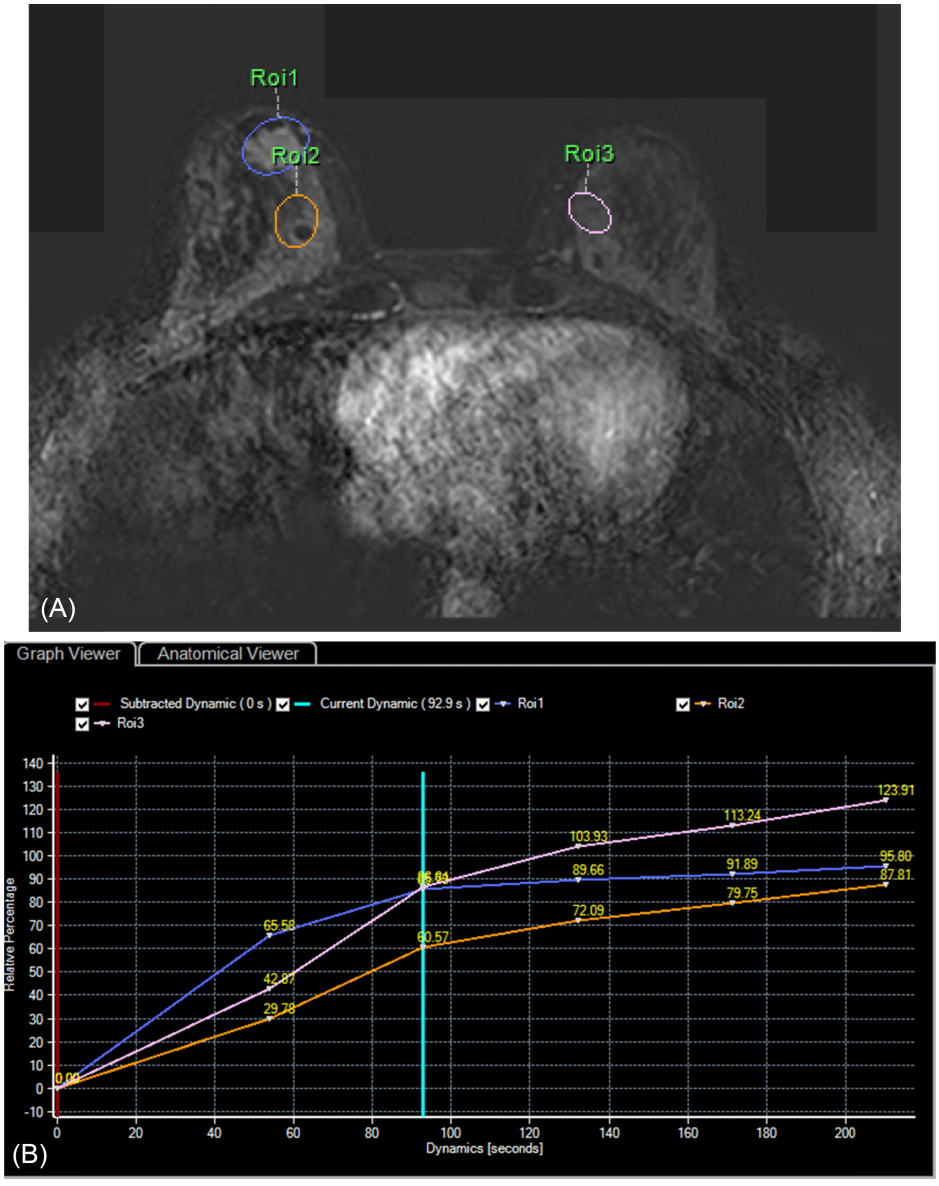

Figure 2 The patient has a mass measuring 32 × 27 mm with a dendritic shaped and spiculated margins in the middle of the right breast and is followingly diagnosed as invasive ductal carcinoma after the biopsy. Histopathological examination reveals estrogen receptor (+), progesterone receptor (−), c-erb B2 (−). A) The mean curve measurement of mass enhancement, non-mass enhancement, and parenchymal enhancement in the contralateral breast on dynamic contrast-enhanced breast MRI using ROI. (B) Displays type 3 enhancement pattern in the time–intensity curve while the non-mass enhancement and the parenchymal enhancement of the contralateral breast are seen as type 2.

metastatic carcinoma in the axillary nodes) was documented in the pathology reports.

Statistical Analysis

All data were analyzed using SPSS v15.0 (SPSS Inc.; Chicago, IL, USA). Descriptive statistics were used to summarize patient demographics, tumor characteristics, and MRI findings. The association between MRI findings (e.g., kinetic curve type, internal enhancement pattern, and background enhancement) and receptor status or molecular subtype was evaluated using the Pearson chi-square test. Similar chi-square analyses were used to assess the relationships between receptor status and other categorical variables, such as lymph node positivity and background enhancement patterns. Differences were considered statistically significant at a P-value < .05.

RESULTS

Patient and Tumor Characteristics

This study included 154 female patients with invasive breast carcinoma (mean age: 51.4 years; range: 24-80). Histopathological analysis identified invasive ductal carcinoma in 96.7% (149/154) and invasive lobular carcinoma (ILC) in 3.3% (5/154) of cases. The MRI BI-RADS categorization classified 63.1% (97/154) of the lesions as BI-RADS 4 (suspicious), 30.5% (49/154) as BI-RADS 5 (highly suggestive of malignancy), and 5.2% (8/154) as BI-RADS 6 (biopsy-proven).

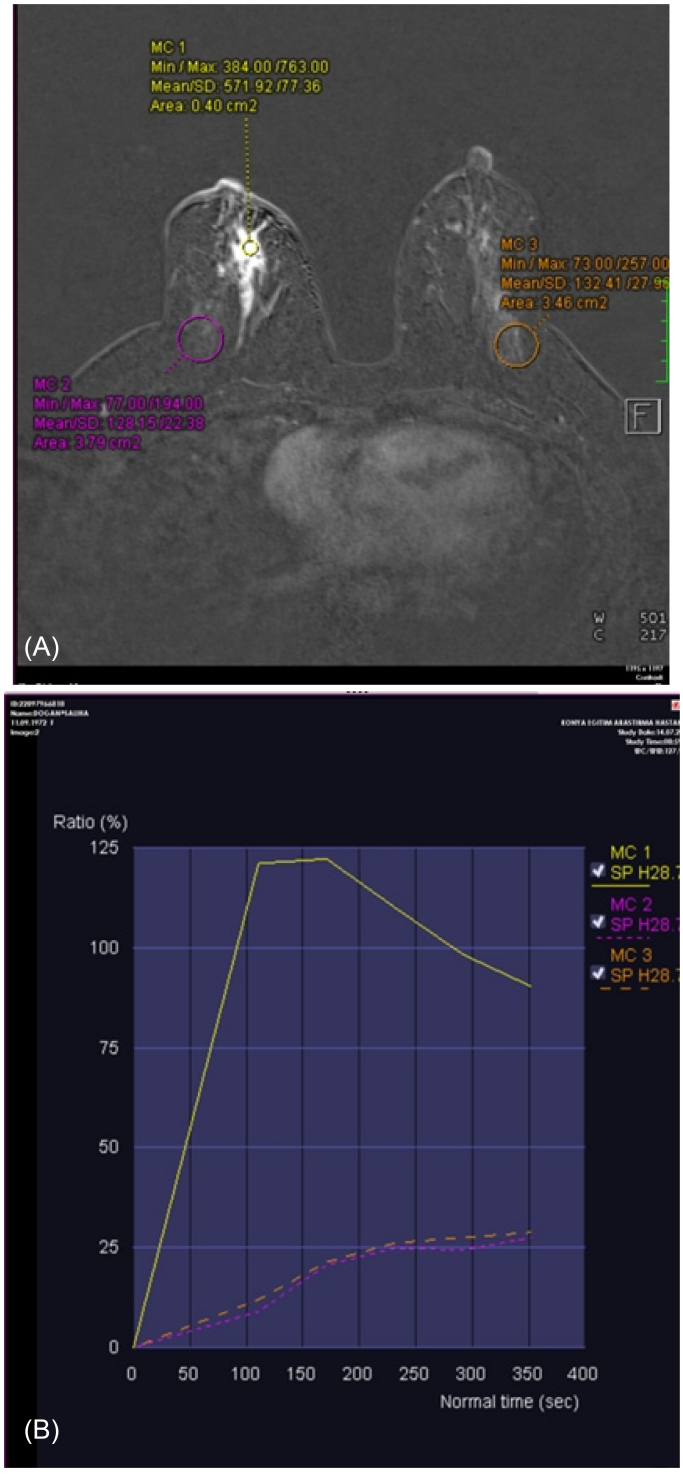

Figure 3 On breast MRI, a 45-year-old female, a mass measuring 15 × 15 mm with linear shape and partly spiculated margins was located in the right breast retroareolar region and was diagnosed as invasive ductal carcinoma according to the biopsy results. (A) The mean curve measurement of mass enhancement, non-mass enhancement, and parenchymal enhancement in the contralateral breast on DCE Breast MRI using ROI. (B) Time–intensity curve displays type 3 mass enhancement pattern, non-mass enhancement, and parenchymal enhancement in the contralateral breast display type 1 pattern.

Tumors were predominantly left-sided (51.9%, 79/154), with bilateral involvement in 1.9% of cases (3/154).

Imaging Features

Morphologically, 56.6% (87/154) of the tumors exhibited irregular shapes (stellate or spiculated), while 43.4% (67/154) were round, oval, or lobulated. Margins were poorly defined or spiculated in 90.9% (140/154) of the lesions. Internal enhancement patterns on DCE-MRI included heterogeneous (40%, 62/154), rim (29%, 45/154), and homogeneous (31%, 47/154) patterns, with rim enhancement frequently observed in high-grade tumors showing central necrosis. Tumor size ranged from 3 mm to 60 mm (mean: 25 mm; median: 20 mm), and multifocal/multicentric disease was present in 54.6% (83/154) of patients.

Molecular Subtype Distribution

Immunohistochemical profiling revealed ER positivity in 39.4% (61/154) of patients, PR positivity in 43.5% (67/154), and HER2 overexpression in 36.4% (56/154). Molecular subtyping categorized tumors as Luminal A (17.4%, 27/154), Luminal B (36.8%, 57/154), or triple-negative (44.5%, 70/154).

Enhancement Kinetics and Statistical Correlations

Contrast enhancement kinetics were classified as type 1 (persistent, 37.7%, 58/154), type 2 (plateau, 36.4%, 56/154), or type 3 (washout, 26.0%, 40/154). Chi-square analysis demonstrated a significant association between Luminal A tumors and type 3 kinetics ($\chi^2 = 4.02$, $P < .05$) (Table 1). Luminal B tumors were correlated with moderate-to-marked BPE (BPE: Type 1 [$\chi^2 = 5.07$] and Type 2 [$\chi^2 = 5.53$], $P < .05$) (Table 2) and contralateral breast enhancement (Table 3). No significant relationships were observed between the molecular subtypes, enhancement patterns, or lymph node metastasis ($P > .05$) (Table 4).

DISCUSSION

This study identified distinct DCE-MRI kinetic and enhancement profiles associated with breast cancer molecular subtypes. Luminal A tumors showed a significant propensity for *Type 3* "washout" kinetics, indicating rapid contrast uptake followed by fast washout. This was an unexpected finding, as classical literature often links Luminal A lesions to more gradual or persistent enhancement pattern.[11] The observation that Luminal A cancers can exhibit aggressive washout curves underscores the heterogeneity of tumor angiogenesis—vascular permeability and perfusion are not determined by receptor status alone, but by the tumor's overall biology. In contrast, Luminal B tumors (were associated in the authors' cohort with moderate-to-marked BPE) and conspicuous contralateral breast enhancement. Luminal B cancers generally have higher proliferation indices (e.g., elevated Ki-67) and often HER2 overexpression, contributing to a more aggressive phenotype. This aggressive biology may manifest on MRI as increased perfusion

Table 1. Contrast Enhancement Pattern vs. Tumor Markers/Subtypes

Tumor Marker/ Subtype	Tip 1 χ^2	*P*	Tip 2 χ^2	*P*	Tip 3 χ^2	*P*
ER	0.00	>.05	0.74	>.05	0.54	>.05
PR	03.09	>.05	0.25	>.05	1.51	>.05
HER2	0.20	>.05	1.29	>.05	1.68	>.05
Triple negative	0.03	>.05	0.28	>.05	0.17	>.05
Luminal A	1.50	>.05	1.13	>.05	04.02	<.05*
Luminal B	0.00	>.05	0.18	>.05	0.10	>.05

ER, estrogen receptor; HER2, human epidermal growth factor receptor 2; PR, progesterone receptor.

Table 2. Background Parenchymal Enhancement vs Tumor Markers/Subtypes

Tumor Marker/Subtype	Tip 1 χ^2	*P*	Tip 2 χ^2	*P*
ER	0.16	>.05	0.23	>.05
PR	0.41	>.05	0.13	>.05
HER2	02.09	>.05	2.45	>.05
Triple negative	1.23	>.05	0.67	>.05
Luminal A	1.52	>.05	1.29	>.05
Luminal B	05.07	<.05*	5.53	<.05*

BPE, background parenchymal enhancement; ER, estrogen receptor; HER2, human epidermal growth factor receptor 2; PR, progesterone receptor.

in surrounding normal tissue, explaining the elevated BPE the authors observed. Prior studies have indeed suggested that more aggressive, higher-grade tumors can induce greater vascularization in adjacent parenchyma.[12]The authors' finding aligns with this concept although the specific association of high BPE with Luminal B subtype is a novel contribution of this study.

The observed association between Luminal A tumors and type 3 (washout) enhancement kinetics in this study presents an intriguing finding that warrants careful interpretation within the context of contemporary literature. Traditionally, washout kinetics have been associated with more aggressive tumor subtypes, particularly triple-negative breast cancer and HER2-enriched tumors.[6] However, recent investigations have revealed increasing complexity in the relationship between enhancement patterns and molecular biology. Blaschke and Abe[13] demonstrated that HER2-positive lesions exhibit significantly greater rapid early contrast uptake compared to luminal subtypes, with 93.8% of HER2+ tumors showing >100% early uptake vs. 77.3% in Luminal A/B tumors ($P < .01$). This apparent discrepancy with the authors' findings may reflect the heterogeneous nature of Luminal A tumors and the influence of various factors including tumor grade, proliferation index, and vascular architecture that can override the typical enhancement patterns associated with hormone receptor status.

The significant correlation between Luminal B tumors and moderate-to-marked BPE observed in this study aligns remarkably well with recent literature and provides important insights into the biological underpinnings of this molecular subtype. Wu et al.[14] established the foundational role of BPE in molecular subtype differentiation through their landmark external validation study, demonstrating that both tumor and BPE characteristics contribute significantly to subtype discrimination with area under the curve (AUC) values ranging from 0.66 to 0.79 across different molecular subtypes. The association between Luminal B tumors and increased BPE likely reflects the more aggressive biological profile of this subtype, characterized by higher proliferation indices (Ki-67) and potential HER2 expression, which may contribute to increased angiogenesis and vascular permeability not only within the tumor but also in the surrounding normal breast tissue.[8] This systemic effect is further supported by the authors' observation of increased contralateral breast enhancement in Luminal B tumors, suggesting a hormonal or growth factor-mediated influence that extends beyond the immediate tumor microenvironment.

Table 3. Contralateral Breast Enhancement vs. Tumor Markers/Subtypes

Tumor Marker/Subtype	Tip 1 χ^2	*P*	Tip 2 χ^2	*P*
ER	0.16	>.05	0.23	>.05
PR	0.07	>.05	0.13	>.05
HER2	02.09	>.05	2.45	>.05
Triple negative	0.62	>.05	0.67	>.05
Luminal A	1.52	>.05	1.29	>.05
Luminal B	05.07	<.05*	5.53	<.05*

ER, estrogen Receptor; HER2, human epidermal growth factor receptor 2; PR, progesterone receptor.

Table 4. Lymph Node Involvement vs. Tumor Markers/Subtypes

Tumor Marker/Subtype	Lymph Node Involvement (LN+) χ^2	*P*
ER	0.00	>.05
PR	1.11	>.05
HER2	0.05	>.05
Triple negative	0.09	>.05
Luminal A	0.02	>.05
Luminal B	0.02	>.05

ER, estrogen receptor; HER2, human epidermal growth factor receptor 2; LN+, positive lymph node involvement; PR, progesterone receptor.

Recent advances in radiomics and artificial intelligence have substantially enhanced the authors' understanding of the relationship between DCE-MRI features and molecular subtypes, providing both validation and expansion of traditional imaging-pathology correlations. Xu et al[15] recently demonstrated that combined intratumoral and peritumoral radiomics signatures based on DCE-MRI can distinguish between luminal and non-luminal breast cancer molecular subtypes with remarkable accuracy, achieving AUC values of 0.956 in training, 0.945 in internal validation, and 0.896 in external validation sets. This multicenter study of 305 patients represents a significant advancement over traditional qualitative assessment methods and provides strong evidence that peritumoral regions contain complementary biological information that enhances molecular subtype prediction. The superior performance of combined intratumoral and peritumoral analysis (AUC 0.896) compared to intratumoral analysis alone (AUC 0.883) supports the concept that tumor biology extends beyond the visible tumor boundaries, influencing the surrounding tissue architecture and vascular characteristics.

The concept of kinetic heterogeneity within breast tumors has emerged as a particularly promising avenue for molecular subtype prediction, as demonstrated by the innovative work of Feng et al[16] who developed a radiomics model based on intra-tumoral kinetic heterogeneity for predicting breast cancer molecular subtypes. Their approach of segmenting tumors into 3 subregions (persistent, washout, and plateau) based on voxel-level contrast enhancement patterns represents a paradigm shift from traditional whole-tumor analysis to region-specific characterization. The superior performance of their washout region model, achieving AUC values of 0.924 for luminal subtype, 0.876 for HER2, and 0.816 for HER2 status prediction, suggests that specific kinetic regions within tumors may harbor more discriminatory information than global tumor characteristics. This finding has particular relevance to this study's observation of washout kinetics in Luminal A tumors, as it suggests that even within traditionally "less aggressive" subtypes, there may be regions of rapid contrast washout that reflect underlying biological heterogeneity and potentially more aggressive tumor components.

The integration of multiparametric MRI approaches has further enhanced the discriminatory power of imaging-based molecular subtype prediction. He et al[17] conducted a comprehensive analysis of 194 breast cancer patients using T2-weighted imaging, diffusion-weighted imaging, and DCE-MRI, employing unsupervised clustering analysis to

identify distinct patient clusters with significant differences in molecular subtypes. Their findings revealed statistically significant differences in Luminal A subtype distribution ($P = .03$), ER status ($P = .01$), PR status ($P = .04$), mean tumor size ($P < .01$), lymph node metastasis ($P = .01$), and edema ($P < .01$) between the identified clusters. This multiparametric approach addresses the limitation of single-sequence analysis and provides a more comprehensive characterization of tumor biology, potentially explaining some of the apparent contradictions in single-parameter studies and supporting the need for integrated imaging biomarkers in clinical practice.

The evolution toward deep learning and artificial intelligence-based approaches has marked a significant milestone in the field of imaging-based molecular subtype prediction. Contemporary studies have demonstrated that deep neural networks can effectively combine DCE-MRI with other imaging modalities to achieve superior performance compared to traditional radiomics approaches.[18] The development of multi-institute deep learning models (MBCNN) for predicting molecular subtypes from DCE-MRI represents a crucial step toward clinical translation, as these models must demonstrate robustness across different imaging protocols, patient populations, and institutional practices. The combination of DCE-MRI with non-mass enhancement diffusion-weighted imaging via deep neural networks has shown particularly promising results, achieving significant improvements in breast cancer molecular subtype prediction compared to either imaging modality alone.[9] This multimodal integration addresses the inherent limitations of single-sequence analysis and provides a more comprehensive assessment of tumor characteristics, including both vascular and cellular properties.

The clinical implications of the authors' findings, when viewed in the context of the broader literature, extend beyond mere academic interest to potential practical applications in personalized breast cancer management. The ability to predict molecular subtypes non-invasively could significantly impact treatment planning, particularly in cases where tissue sampling is challenging or when assessing tumor heterogeneity across large lesions. However, several important limitations must be acknowledged. The authors' study's retrospective design and single-center nature limit the generalizability of findings, particularly given the demonstrated importance of external validation in imaging biomarker studies.[14] The relatively small number of patients in certain molecular subtype categories, particularly HER2-enriched tumors, may have limited the authors' ability to detect significant associations and contributed to the apparent discrepancies with some literature findings. Furthermore, the evolution of molecular subtyping criteria over time, including the recent recognition of HER2-low tumors as a distinct entity,[19] highlights the dynamic nature of breast cancer classification and the need for imaging biomarkers to adapt accordingly.

The absence of significant associations between molecular subtypes and lymph node metastasis in this study is consistent with multiple contemporary investigations and reflects the complex, multifactorial nature of metastatic spread in breast cancer.[20] This finding suggests that while DCE-MRI characteristics may effectively predict molecular subtypes, they may not be sufficient predictors of nodal involvement, which depends on additional factors including tumor size, histological grade, lymphovascular invasion, and proliferative rate. Recent large-scale multicenter studies have confirmed this limitation, with a comprehensive analysis of 1506 pre-treatment DCE-MRI cases demonstrating that imaging features alone are insufficient for reliable lymph node status prediction.[21] This limitation underscores the importance of integrating imaging biomarkers with clinical and pathological factors rather than relying on imaging characteristics in isolation.

Overall, this study highlights that DCE-MRI kinetic data and internal enhancement patterns can provide important insights into the molecular subtypes of breast cancer. It is worth noting that the distribution of molecular subtypes in this study differs from most population-based reports, where Luminal A is typically the most prevalent form of breast cancer. In the authors' series, Luminal A tumors accounted for only 17.4% of cases, while Luminal B and triple-negative subtypes were more frequent. Several factors may explain this discrepancy. First, as a tertiary oncology center, the authors' institution receives a disproportionate number of aggressive or diagnostically complex cases, potentially leading to selection bias. Second, the retrospective nature of this study limited the availability of proliferation index data (Ki-67), which is essential for accurately distinguishing between Luminal A and Luminal B subtypes. Consequently, some ER/PR-positive tumors with unknown or high proliferation rates may have been classified as Luminal B by default. Third, partial or low-level hormone receptor expression (e.g., ER or PR just above the 1% cutoff) may not correlate with classical Luminal A biology. These limitations likely contributed to the lower observed prevalence of Luminal A and should be considered when interpreting subtype-specific imaging patterns. However, the generalizability of these findings should be approached cautiously given the limited number of patients in certain subgroups (e.g., HER2-enriched) and the retrospective nature of the study. Differences in DCE-MRI protocols between centers, along with variability among readers, are further limitations that should be considered.

Future directions in this field are likely to focus on several key areas that address current limitations and expand clinical applicability. The standardization of DCE-MRI protocols across institutions represents a critical need, as variations in imaging parameters, contrast agents, and acquisition techniques can significantly impact radiomics feature extraction and model performance.[22] The development of federated learning approaches may enable the creation of robust, generalizable models while preserving patient privacy and institutional autonomy. Additionally, the integration of imaging biomarkers with genomic data through radiogenomics approaches holds promise for developing more comprehensive predictive models that capture both phenotypic and genotypic tumor characteristics.[23] The recent emergence of time-dependent diffusion MRI as an effective method for molecular subtype prediction[24] suggests that novel imaging techniques may provide complementary information to traditional DCE-MRI approaches, potentially improving overall predictive accuracy.

In conclusion, this study contributes to the evolving understanding of DCE-MRI characteristics in breast cancer molecular subtype prediction, while highlighting both the potential and limitations of current imaging-based approaches. The significant association between Luminal A tumors and washout kinetics, though seemingly contradictory to traditional expectations, may reflect the biological heterogeneity within molecular subtypes and the need for more sophisticated analytical approaches. The consistent association between Luminal B tumors and increased BPE across multiple studies suggests a robust biological relationship that may have clinical utility. As the field moves toward increasingly sophisticated artificial intelligence and radiomics approaches, the integration of multiple imaging parameters, external validation across diverse populations, and standardization of protocols will be essential for translating these research findings into clinically applicable tools. The ultimate goal remains the development of

comprehensive, non-invasive imaging biomarkers that can guide personalized treatment decisions and improve outcomes for breast cancer patients worldwide

Data Availability Statement: The data that support the findings of this study are available on request from the corresponding author.

Ethics Committee Approval: Ethics committee approval was received for this study from the ethics committee of Konya Necmettin Erbakan University (Approval No: 2214/5 Date: 20.01.2016).

Informed Consent: Given the retrospective design of the study, the requirement for informed consent was waived by the ethics committee.

Peer-review: Externally peer reviewed.

Author Contributions: Concept – A.F.T.; Design – A.F.T.; Supervision – S.Ö., İ.T.; Resources – A.F.T.; Materials – A.F.T.; Data Collection and/or Processing – A.F.T.; Analysis and/or Interpretation – A.F.T.; Literature Search – Y.C.K., V.T.; Writing Manuscript – A.F.T.; Critical Review –S.Ö., İ.T.; Other – İ.T.

Declaration of Interests: The authors have no conflict of interest to declare.

Funding: The authors declared that this study has received no financial support.

REFERENCES

1. Perou CM, Sørlie T, Eisen MB, et al. Molecular portraits of human breast tumors. *Nature*. 2000;406(6797):747-752. [CrossRef]
2. Kuhl CK, Schrading S, Bieling HB, et al. MRI for diagnosis of pure ductal carcinoma in situ: a prospective observational study. *Lancet*. 2007;370(9586):485-492. [CrossRef]
3. Mann RM, Kuhl CK, Kinkel K, Boetes C. Breast MRI: guidelines from the European Society of Breast Imaging. *Eur Radiol*. 2008;18(7):1307-1318. [CrossRef]
4. Nielsen T, Wittenborn T, Horsman MR. Dynamic contrastenhanced magnetic resonance imaging (DCEMRI) in preclinical studies of antivascular treatments. *Pharmaceutics*. 2012;4(4):563-589. [CrossRef]
5. Tajima CC, Arruda FPSG, Mineli VC, et al. MRI features of breast cancer immunophenotypes with a focus on luminal estrogen receptor low–positive invasive carcinomas. *Sci Rep*. 2024;14(1):19305. [CrossRef]
6. Uematsu T, Kasami M, Yuen S. Triplenegative breast cancer: correlation between MR imaging and pathologic findings. *Radiology*. 2009;250(3):638-647. [CrossRef]
7. Holli-Helenius K, Salminen A, Rinta-Kiikka I, et al. MRI texture analysis in differentiating luminal A and luminal B breast cancer molecular subtypes—a feasibility study. *BMC Med Imaging*. 2017;17(1):69. [CrossRef]
8. Dilorenzo G, Telegrafo M, La Forgia D, Stabile Ianora AA, Moschetta M. Breast MRI background parenchymal enhancement as an imaging bridge to molecular cancer subtype. *Eur J Radiol*. 2019;113:148-152. [CrossRef]
9. Erguvan-Dogan B, Whitman GJ, Kushwaha AC, Phelps MJ, Dempsey PJ. BIRADSMRI: a primer. *AJR Am J Roentgenol*. 2006;187(2):W15 2-W160. [CrossRef]
10. Rakha EA, Starczynski J, Lee AHS, Ellis IO. The updated ASCO/CAP guideline recommendations for HER2 testing in the management of invasive breast cancer: a critical review of their implications for routine practice. *Histopathology*. 2014;64(5):609-615. [CrossRef]
11. Szep M, Pintican R, Boca B, et al. Multiparametric MRI features of breast cancer molecular subtypes. *Medicina (Kaunas)*. 2022;58(12):1716. [CrossRef]
12. Wei Z, Chen X, Yang Y, Yang L, Ma X. The potential role of breast MRI in evaluation of triplenegative breast cancer and fibroadenoma of less than 3 cm. *Transl Cancer Res*. 2024;13(8):4042-4051. [CrossRef]
13. Blaschke E, Abe H. MRI phenotype of breast cancer: kinetic assessment for molecular subtypes. *J Magn Reson Imaging*. 2015;42(4):920-924. [CrossRef]
14. Wu J, Sun X, Wang J, et al. Identifying relations between imaging phenotypes and molecular subtypes of breast cancer: model discovery and external validation. *J Magn Reson Imaging*. 2017;46(4):1017-1027. [CrossRef]
15. Xu H, Yang A, Kang M, et al. Intratumoral and peritumoral radiomics signature based on DCEMRI can distinguish between luminal and nonluminal breast cancer molecular subtypes. *Sci Rep*. 2025;15(1):14720. [CrossRef]
16. Feng S, Yin J. Dynamic contrastenhanced magnetic resonance imaging radiomics analysis based on intratumoral subregions for predicting luminal and nonluminal breast cancer. *Quant Imaging Med Surg*. 2023;13(10):6735-6749. [CrossRef]
17. He Y, Duan S, Wang W, et al. Integrative radiomics clustering analysis to decipher breast cancer heterogeneity and prognostic indicators through multiparametric MRI. *npj Breast Cancer*. 2024;10(1):72. [CrossRef]
18. Ba ZC, Zhang HX, Liu AY, et al. Combination of DCEMRI and NMEDWI via deep neural network for predicting breast cancer molecular subtypes. *Clin Breast Cancer*. 2024;24(5):e417-e427. [CrossRef]
19. Yin L, Zhang Y, Wei X, et al. Preliminary study on DCEMRI radiomics analysis for differentiation of HER2low and HER2zero breast cancer. *Front Oncol*. 2024;14:1385352. [CrossRef]
20. Turnbull LW. Dynamic contrastenhanced MRI in the diagnosis and management of breast cancer. *NMR Biomed*. 2009;22(1):28-39. [CrossRef]
21. Garrucho L, Kushibar K, Reidel CA, et al. A largescale multicenter breast cancer DCEMRI benchmark dataset with expert segmentations. *Sci Data*. 2025;12(1):453. [CrossRef]
22. Qi YJ, Su GH, You C, et al. Radiomics in breast cancer: current advances and future directions. *Cell Rep Med*. 2024;5(9):101719. [CrossRef]
23. You C, Su GH, Zhang X, et al. Multicenter radiomultiomic analysis for predicting breast cancer outcome and unraveling imagingbiological connection. *NPJ Precis Oncol*. 2024;8(1):193. [CrossRef]
24. Wang X, Ba R, Huang Y, et al. Timedependent diffusion MRI helps predict molecular subtypes and treatment response to neoadjuvant chemotherapy in breast cancer. *Radiology*. 2024;313(1):e240288. [CrossRef]

Current Research in MRI

Original Article

Fast Magnetic Resonance Diffusion-Weighted Imaging Versus Computed Tomography in Diagnosis of Hyperacute Ischemic Stroke

Saleem Khadir Musalah[1,2]

[1]Department of Surgery, University of Duhok College of Medicine, Duhok, Iraq
[2]Department of Radiology, Azadi Teaching Hospital, Duhok, Iraq

Cite this article as: Musalah SK. Fast magnetic resonance diffusion-weighted imaging versus computed tomography in diagnosis of hyperacute ischemic stroke. *Current Research in MRI*, 2025;4(2):35-38.

Corresponding author: Saleem Khadir Musalah, e-mail: Saleem.musalah@uod.ac

Received: August 29, 2025 **Accepted:** September 22, 2025 **Publication Date:** October 30, 2025

DOI: 10.5152/CurrResMRI.2025.25124

Abstract

Objective: Hyperacute ischemic stroke is a time-critical emergency that requires rapid and accurate diagnosis to enable timely intervention and improve outcomes. While non-contrast computed tomography (CT) is commonly used for initial evaluation due to its availability and speed, it has limited sensitivity for early ischemic changes, particularly in posterior circulation strokes. This study aimed to compare the diagnostic performance of fast diffusion-weighted imaging (DWI) and CT in the detection of hyperacute ischemic stroke within 6 hours of symptom onset.

Methods: This prospective cross-sectional study included 72 patients presenting to Azadi Teaching Hospital, Duhok, between June and November 2024 with acute stroke symptoms. After excluding hemorrhage via non-contrast CT, eligible patients underwent DWI within 6 hours of symptom onset. Demographic, clinical, and imaging data were recorded and analyzed using SPSS.

Results: Among the 72 patients (mean age 64.7 years; 51.4% male), all underwent DWI within a mean of 3.2 hours from symptom onset. Left-sided infarctions were most common (62.8%), followed by right-sided (31.9%) and bilateral lesions (4.1%). The middle cerebral artery was the most frequently affected territory (58.3%). Hypertension was the most prevalent risk factor (63.8%), followed by diabetes (44.4%) and heart disease (37.5%). Diffusion-weighted imaging detected acute ischemic lesions in 100% of patients, whereas CT detected lesions in only 37.5%. Computed tomography was particularly limited in detecting posterior circulation strokes.

Conclusion: Diffusion-weighted imaging demonstrated superior sensitivity compared to CT in the diagnosis of hyperacute ischemic stroke, particularly for posterior fossa lesions. These findings support the adoption of magnetic resonance imaging–first imaging protocols in acute stroke settings. The establishment of a stroke management center in Duhok was recommended to facilitate rapid diagnosis and evidence-based care.

Keywords Acute ischemic stroke, CT, fast diffusion-weighted imaging, hyperacute stroke

INTRODUCTION

Stroke is one of the leading causes of mortality and long-term disability worldwide, posing a significant public health burden.[1] Clinically, stroke refers to a sudden onset of neurological deficit due to a vascular cause,[2] broadly classified into hemorrhagic (15%-25%) and ischemic types (75%-85%).[3] Among these, ischemic stroke demands particularly swift intervention, as therapeutic efficacy, especially for reperfusion strategies, is highly time-dependent.[4] Early and accurate diagnosis within the hyperacute phase, defined as the first 6 hours from symptom onset, is critical for initiating effective treatment and improving patient outcomes.[5]

Conventional imaging with non-contrast computed tomography (NCCT) remains the first-line modality in many centers due to its availability and utility in ruling out hemorrhage.[6] However, CT is known to have limited sensitivity for detecting early ischemic changes. The sensitivity of CT for infarction has been reported to be as low as 30% at 3 hours and approximately 60% at 24 hours.[7,8]

In contrast, magnetic resonance imaging (MRI), particularly diffusion-weighted imaging (DWI), has emerged as a highly sensitive tool for identifying hyperacute ischemic changes.[9] Diffusion-weighted imaging can reveal cytotoxic edema within minutes of onset as hyperintense lesions with corresponding apparent diffusion coefficient (ADC) hypointensity, allowing for early and accurate diagnosis.[10] Comparative imaging studies consistently demonstrate DWI's superiority over NCCT in sensitivity and accuracy, especially for middle cerebral artery (MCA) territory infarction.[11]

Recent developments have fueled interest in MRI-first imaging protocols, even in the hyperacute window. Evidence suggests that MRI-based pathways can be implemented in comprehensive stroke centers with minimal delay and significantly improved diagnostic yield compared to CT-first workflows.[12] Furthermore, advanced diffusion and perfusion imaging markers—such as Diffusion-Weighted Imaging–Alberta Stroke Program Early CT Score(DWI-ASPECTS), lesion volume, and perfusion metrics—have emerged as important predictors of final infarct size and functional outcomes.[13]

Despite technological advances, NCCT remains the mainstay in many healthcare settings due to its accessibility and speed, particularly in settings with limited MRI availability. Limitations include low sensitivity for posterior circulation strokes, early small infarcts, and inter-reader variability in detecting early ischemic signs.[14] Artificial intelligence (AI)–supported algorithms applied to NCCT have shown promise in improving detection of early ischemic changes, although performance remains variable, especially for small infarcts.[15]

Taken together, there is a pressing need for robust comparative assessment of NCCT versus fast DWI protocols in real-world hyperacute stroke settings. Such studies should assess not only diagnostic sensitivity and specificity but also the relationship between imaging findings (e.g., DWI lesion volume, DWIASPECTS) and clinical variables such as NIHSS and functional outcome (e.g., mRS).[16,5]

This study aims to evaluate the diagnostic performance of fast DWI compared to NCCT in the detection of hyperacute ischemic stroke within 6 hours of symptom onset. By focusing on a local clinical population, the aim was to assess the applicability of advanced imaging protocols in real-world settings, potentially contributing to optimized stroke management in the region.

MATERIAL AND METHODS

Ethics Committee Approval

This research was performed in compliance with the revised Declaration of Helsinki and received approval from the Institutional Ethics Committee of the University of Duhok on July 17, 2022 (Institutional Review Board Approval Number: DDG N. 13062022-7-17).

All participants provided informed consent before being included in the study; data was anonymized to protect donor confidentiality**.**

Study Design and Setting

A cross-sectional, prospective diagnostic accuracy study was conducted at the Emergency and Radiology Departments of Azadi Teaching Hospital, affiliated with the College of Medicine, University of Duhok, Iraq. The study period spanned from June 1 to November 1, 2024.

Study Population

A total of 72 patients with suspected hyperacute ischemic stroke were consecutively enrolled. Inclusion criteria comprised patients presenting with acute focal neurological deficits consistent with ischemic stroke within 6 hours of symptom onset. All patients underwent an initial NCCT scan to exclude intracerebral hemorrhage. Patients with confirmed hemorrhage on NCCT were excluded from the study.

MAIN POINTS

- Diffusion-weighted magnetic resonance imaging (MRI) detected hyperacute ischemic stroke lesions in 100% of patients, while computed tomography (CT) identified only 37.5%, confirming the superior sensitivity of diffusion-weighted imaging (DWI).
- Diffusion-weighted imaging proved especially effective in identifying posterior fossa infarctions, where CT sensitivity was markedly low.
- Hypertension, diabetes, and heart disease were the most common risk factors in this cohort, aligning with established stroke epidemiology.
- Findings support adopting MRI-first protocols in acute stroke management, with potential to improve early diagnosis and patient outcomes in resource-equipped centers.

Imaging Protocol

Following exclusion of hemorrhage, all patients underwent fast MRI with DWI on either a 1.5 Tesla or 3 Tesla MRI scanner, within the hyperacute window (≤6 hours post-symptom onset). Diffusion-weighted imaging images were evaluated alongside ADC maps to confirm ischemic lesions. Computed tomography scans were performed using a standard multislice CT scanner and interpreted by an experienced radiologist blinded to the MRI findings. The sensitivity of NCCT in detecting early ischemic changes was compared to DWI, which was considered the reference standard due to its established diagnostic superiority in hyperacute stroke.

Data Collection and Variables

Demographic data (age, sex), time from symptom onset to imaging, side and vascular territory of infarction (e.g., MCA, vertebrobasilar circulation), and risk factors (e.g., hypertension, diabetes mellitus, heart disease, smoking, obesity, and family history) were recorded using a standardized data collection sheet.

Imaging Analysis

Diffusion-weighted imaging positivity was defined as hyperintense signal on DWI with corresponding hypointensity on ADC maps. Computed tomography positivity was defined by the presence of visible hypodensity, loss of gray-white matter differentiation, or other early signs of ischemia. Imaging findings were categorized by side (right, left, bilateral) and vascular territory.

Stroke Classification

Ischemic strokes were categorized based on the time from symptom onset into 4 stages: hyperacute (0-6 hours), acute (6-24 hours), subacute (1-14 days), and chronic (>14 days), following previously established imaging criteria[17,18]

Each stage demonstrates characteristic changes on DWI and ADC sequences. Table 1 summarizes the expected signal changes in DWI and ADC across these time intervals.

Statistical Analysis

Data analysis was performed using SPSS version 10 (SPSS Inc.; Chicago, IL, USA). Descriptive statistics (mean, SD, percentages) were used for demographic and clinical variables. Sensitivity and detection rates for DWI and CT were calculated. A P-value ≤ .05 was considered statistically significant. The clinical diagnosis based on presentation was used as the reference standard for sensitivity comparison.

RESULTS

Age and Sex Distribution

A total of 72 patients with suspected hyperacute ischemic stroke were included in this study. The mean age was 64.7 years (range: 17-86 years). Of the total, 37 patients (51.4%) were male and 35 (48.6%) were female. All patients were assessed within 6 hours of symptom onset, with an average time of 3.2 hours from onset to imaging (Table 2).

Table 1. Changes in Diffusion-Weighted Imaging and Apparent Diffusion Coefficient Findings by Time

Time	<6 Hours	3 Days	7 Days	30 Days
DWI	Bright	Very bright	Bright	Isointense
ADC	Dark	Very dark	Dark	Bright

ADC, apparent diffusion coefficient; DWI, diffusion-weighted imaging.

Table 2. Gender and Lesion Side Distribution

Variable		Number	%
Gender	Male	37	51.4
	Female	35	48.6
Lesion side	Right	23	31.9
	Left	46	63.8
	Bilateral	3	4.1

Lesion Distribution

Regarding lesion laterality, infarction was more commonly observed in the left hemisphere, affecting 46 patients (62.8%), while right-sided lesions were found in 23 patients (31.9%). Only 3 patients (4.1%) exhibited bilateral involvement (Table 2).

Vascular Territory Involvement

The most frequently affected vascular territory was the MCA, observed in 42 patients (58.3%). The vertebrobasilar system was involved in 20 patients (27.8%). Combined anterior and MCA involvement was recorded in 5 patients (6.9%), middle and posterior cerebral arteries in 3 patients (4.2%), and isolated anterior cerebral artery infarction in 2 patients (2.8%) (Table 3).

Risk Factors

Hypertension was the most prevalent risk factor, affecting 46 patients (63.8%). Other common comorbidities included diabetes mellitus in 32 patients (44.4%), heart disease in 27 (37.5%), smoking in 19 (26.3%), and obesity in 15 (20.8%). A family history of stroke was reported in 13 patients (18.0%) (Table 4).

Imaging Findings

All 72 patients underwent both non-contrast CT and DWI. Diffusion-weighted imaging successfully identified acute ischemic lesions in all patients (100%), while CT detected ischemic changes in only 27 cases (37.5%). Thus, 45 patients (62.5%) had false-negative CT results despite clear evidence of infarction on DWI. The difference in lesion detection between CT and DWI was statistically significant ($P < .001$). Importantly, DWI was particularly superior in detecting posterior circulation strokes. Of the 29 patients with infarcts involving the posterior fossa, only 5 (17.2%) were identified by CT, while all were visualized on DWI.

DISCUSSION

In this diagnostic accuracy study, DWI reliably identified ischemic lesions in 100% of patients presenting within 6 hours of symptom onset, while CT detected lesions in only 37.5%, underscoring a substantial sensitivity gap in favor of DWI. These results corroborate longstanding findings demonstrating the superior diagnostic accuracy of DWI in hyperacute stroke detection.[19,20]

Recent studies reinforce this paradigm shift. A meta-analysis confirms that even CT protocols enhanced with perfusion imaging significantly underperform compared to DWI in detecting early ischemic changes.[21] Moreover, emerging evidence supports the practicality of MRI-first protocols in acute stroke workflows. A multicenter investigation demonstrates that even ultrafast MRI with concurrent Magnetic Resonance Angiography(MRA), performed in as little as 3 minutes, maintains diagnostic sensitivity comparable to standard MRI in identifying vessel occlusions and ischemic lesions.[22]

Deep-learning–accelerated MRI acquisition techniques offer further promise. One study reported that rapid MRI protocols using AI reconstruction yielded images equivalent in quality to conventional scans—while reducing scan time by up to 75%—without sacrificing lesion detection capability.[23] These findings address one of the primary concerns cited against MRI-first approaches: scan-to-treatment delay.

In addition to technical superiority, DWI provides prognostic insight. A systematic review and meta-analysis indicates that DWI-negative presentations occur in approximately 11%-16% of stroke patients, especially in mild or posterior circulation strokes, and are associated with better functional outcomes (e.g., mRS 0-1), lower recurrence rates, and reduced mortality.[12,19]

In this cohort, CT underperformed particularly in detecting posterior fossa lesions (only 5 of 29 cases), while DWI detected all, reinforcing its critical role in evaluating vertebrobasilar infarction.

Despite MRI's superior sensitivity and prognostic value, CT remains ubiquitous—particularly in resource-limited settings. However,

Table 3. Study Sample by Arterial Territory

Arterial Territory	Numbers	%
Middle cerebral artery	42	58.33
Vertebral basilar arteries	20	27.77
Anterior and middle cerebral artery	5	6.94
Middle and posterior cerebral artery	3	4.16
Anterior cerebral artery	2	2.77

Table 4. Study Sample by Risk Factors

Risk Factors	Stroke Patients with Risk Factors	%
Hypertension	46	63.8
DM	32	44.4
Heart disease	27	37.5
Smoking	19	26.3
Obesity	15	20.8
Family history	13	18

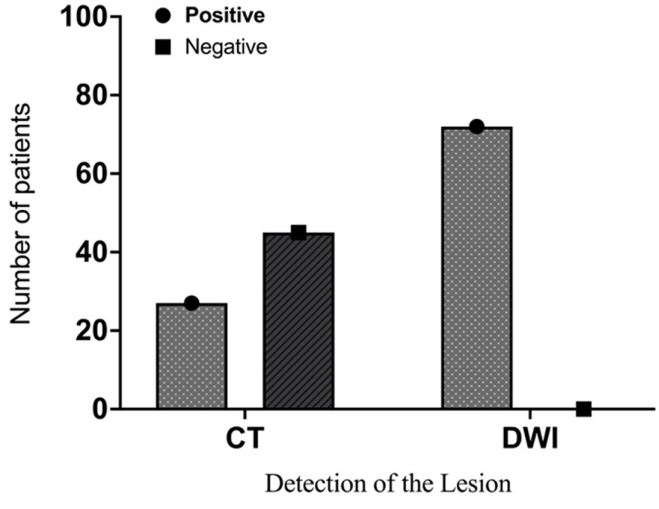

Figure 1. The bar graph illustrating lesion detection rates by computed tomography (CT) versus diffusion-weighted imaging (DWI). It clearly shows that DWI identified lesions in all 72 patients, while CT detected lesions in only 27, missing 45 cases.

recent position statements, including from the American Academy of Neurology, now recommend DWI-based imaging over CT as the preferred first-line modality in acute ischemic stroke assessment.[24]

These findings support adopting MRI-first protocols in acute stroke imaging workflows where infrastructure permits. Integration of 3-minute ultrafast MRI or 6-minute MRI code stroke protocols, paired with AI-based reconstruction and deep-learning segmentation, can significantly reduce door-to-imaging times without compromising diagnostic accuracy.[22] Tele-stroke and remote MRI interpretation systems could further expand access in underserved regions. Although this study did not observe any DWI-negative strokes, prior literature indicates that such cases, though uncommon—can occur, particularly in mild or posterior circulation strokes. In these situations, clinical management still critically depends on clinical evaluation and risk factor assessment.

Limitations include modest sample size, single-center design, and limited availability of advanced imaging such as perfusion MRI or CT perfusion. Future studies incorporating perfusion-diffusion mismatch evaluation using arterial spin labeling or dynamic susceptibility contrast MRI could refine core-penumbra assessment in early stroke management.

In conclusion, DWI-MRI offers unquestionable advantages over NCCT in the detection of hyperacute ischemic stroke, especially in lesions affecting the posterior circulation. Emerging fast MRI protocols and AI-supported workflows have the potential to eliminate previous logistical barriers to MRI-first paradigms. In settings where MRI is available and properly implemented, standard of care should increasingly favor DWI-based assessment over CT in acute stroke—aligning radiologic practice with evolving international guidelines.

Data Availability Statement: The data that support the findings of this study are available on request from the corresponding author.

Ethics Committee Approval: Ethical committee approval was received from the Ethics Committee of University of University of Duhok (Approval No: 13062022-7-17; Date: July 17, 2022).

Informed Consent: Written informed consent was obtained from the participants who agreed to take part in the study.

Peer-review: Externally peer-reviewed.

Declaration of Interests: The author has no conflict of interest to declare.

Funding: The author declared that this study has received no financial support.

REFERENCES

1. Katan M, Luft A. Global burden of stroke. *Semin Neurol*. 2018;38(2):208-211. [CrossRef]
2. Murphy SJ, Werring DJ. Stroke: causes and clinical features. *Medicine (Abingdon)*. 2020;48(9):561-566. [CrossRef]
3. Perna R, Temple J. Rehabilitation Outcomes: ischemic versus hemorrhagic Strokes. *Behav Neurol*. 2015;2015:891651. [CrossRef]
4. Ospel JM, Holodinsky JK, Goyal M. Management of acute ischemic stroke due to large-vessel occlusion: JACC focus seminar. *J Am Coll Cardiol*. 2020;75(15):1832-1843. [CrossRef]
5. Patil S, Rossi R, Jabrah D, Doyle K. Detection, diagnosis and treatment of acute ischemic stroke: current and future perspectives. *Front Med Technol*. 2022;4:748949. [CrossRef]
6. Vanhoenacker P. CT diagnosis of acute bleeding. *JBSR*. 2023;107(1):98. [CrossRef]
7. Abdalkader M, Siegler JE, Lee JS, et al. Neuroimaging of acute ischemic stroke: multimodal imaging approach for acute endovascular therapy. *J Stroke*. 2023;25(1):55-71. [CrossRef]
8. Gao J, Parsons MW, Kawano H, et al. Visibility of CT early ischemic change is significantly associated with time from stroke onset to baseline scan beyond the first 3 hours of stroke onset. *J Stroke*. 2017;19(3):340-346. [CrossRef]
9. Vert C, Parra-Fariñas C, Rovira À. MR imaging in hyperacute ischemic stroke. *Eur J Radiol*. 2017;96:125-132. [CrossRef]
10. Dmytriw AA, Sawlani V, Shankar J. Diffusion-weighted imaging of the brain: beyond stroke. *Can Assoc Radiol J*. 2017;68(2):131-146. [CrossRef]
11. Hwang DY, Silva GS, Furie KL, Greer DM. Comparative Sensitivity of Computed Tomography vs. magnetic resonance imaging for Detecting Acute Posterior fossa Infarct. *J Emerg Med*. 2012;42(5):559-565. [CrossRef]
12. Rapillo CM, Dunet V, Pistocchi S, et al. Moving from CT to MRI paradigm in acute ischemic stroke: feasibility, effects on stroke diagnosis and long-term outcomes. *Stroke*. 2024;55(5):1329-1338. [CrossRef]
13. Pei C, He C, Li H, et al. Clinical and imaging markers for the prognosis of acute ischemic stroke. *Front Neurol*. 2024;15:1345914. [CrossRef]
14. Arif KA, Florian IS, Florian AI, Blesneag AV, Maer E, Chereches RM. Assessing acute DWI lesions in clinically diagnosed TIA: insights from a cohort study in Cluj, Romania. *Tomography*. 2025;11(4):40. [CrossRef]
15. Mohapatra S, Lee TH, Sahoo PK, Wu CY. Localization of early infarction on non-contrast CT images in acute ischemic stroke with deep learning approach. *Sci Rep*. 2023;13(1):19442. [CrossRef]
16. Mortimer AM, Simpson E, Bradley MD, Renowden SA. Computed tomography angiography in hyperacute ischemic stroke: prognostic implications and role in decision-making. *Stroke*. 2013;44(5):1480-1488. [CrossRef]
17. Moritani T, Smoker WRK, Sato Y, Numaguchi Y, Westesson PLA. Diffusion-weighted imaging of acute excitotoxic brain injury. *AJNR Am J Neuroradiol*. 2005;26(2):216-228.
18. Kim HJ, Choi CG, Lee DH, Lee JH, Kim SJ, Suh DC. High-b-value diffusion-weighted MR imaging of hyperacute ischemic stroke at 1.5T. *AJNR Am J Neuroradiol*. 2005;26(2):208-215.
19. Alkhiri A, Alturki F, Alansari NM, et al. Prognosis and distribution of ischemic stroke with negative diffusion-weighted imaging: a systematic review and meta-analysis. *Front Neurol*. 2024;15:1376439. [CrossRef]
20. González RG, Schaefer PW, Buonanno FS, et al. Diffusion-weighted MR imaging: diagnostic accuracy in patients imaged within 6 hours of stroke symptom onset. *Radiology*. 1999;210(1):155-162. [CrossRef]
21. Cviková M, Haršány M, Vinklárek J, Štefela J, Fojtová I, Mikulík R. Effectiveness of computed tomography perfusion imaging in stroke management. *Front Neurol*. 2024;15:1390501. [CrossRef]
22. Cortes-Albornoz MC, Clifford B, Lo WC, et al. A 3-minute ultrafast MRI and MRA protocol for screening of acute ischemic stroke. *J Am Coll Radiol*. 2025;22(3):366-375. [CrossRef]
23. Altmann S, Grauhan NF, Brockstedt L, et al. Ultrafast brain MRI with deep learning reconstruction for suspected acute ischemic stroke. *Radiology*. 2024;310(2):e231938. [CrossRef]
24. Schellinger PD, Bryan RN, Caplan LR, et al. Evidence-based guideline: the role of diffusion and perfusion MRI for the diagnosis of acute ischemic stroke [RETIRED]: report of the Therapeutics and Technology Assessment Subcommittee of the American Academy of Neurology. *Neurology*. 2010;75(2):177-185. [CrossRef]

Current Research in MRI

Original Article

Craniocervical Junction Measurements and Analyses on Age and Gender Differences Using Magnetic Resonance Imaging

Berihat Kızılgöz[1], Muhammet Fırat Öztepe[2]

[1]Republic of Türkiye, Ministry of Health, Provincial Health Directorate, Community Health Center, Erzincan, Türkiye
[2]Department of Radiology, , Erzincan Binali Yıldırım University Faculty of Medicine, Erzincan, Türkiye

Cite this article as: Kızılgöz B, Öztepe MF. Craniocervical junction measurements and analyses on age and gender differences using magnetic resonance imaging. *Current Research in MRI*, 2025;4(2):39-44.

Corresponding author: Berihat Kızılgöz, e-mail: berihatkizilgoz@gmail.com

Received: August 5, 2025 **Revision Requested:** September 8, 2025 **Last Revision Received:** September 8, 2025 **Accepted:** September 22, 2025 **Publication Date:** October 30, 2025

DOI: 10.5152/CurrResMRI.2025.25125

Abstract

Objective: The purpose of this research was verifying the mean values and ranges of powers ratio (PR), atlanto-dental interval (ADI), basion-dens interval (BDI), and basion-axial interval (BAI) which are critical measurements to evaluate atlantooccipital and atlantoaxial dissociations which indicate instability of the injuries in these critical regions.

Methods: After exclusions, 184 female, 87 male, a total of 271 patients' (the mean age was 48.44 ± 14.99) cervical magnetic resonance images were re-assessed regarding the craniocervical measurements. The mean values and SDs of all parameters were presented. All data distribution results of each ratio and interval measurements were presented with boxplot graphics. Each parameter was analyzed regarding gender differences and age.

Results: The mean values of PR, ADI, BDI, and BAI were 0.76 ± 0.07, 1.14 ± 0.61, 5.12 ± 1.74, and 7.41 ± 2.20 respectively. Female and male groups indicated a significant difference regarding ADI and BDI measurements. A significant and negative correlation with ADI and BDI was found regarding age.

Conclusion: Besides the mean values and ranges of the 4 critically important parameters, males had higher ADI and BDI values than females, and age showed a negative significant correlation regarding ADI and BDI measurements according to the results of this investigation. More studies and data from larger series need to be added to the literature to create accurate and valuable meta-analyses that will reveal the normal ranges of these critical values and the effect of age and gender on these parameters.

Keywords: Cervical, Craniocervical junction, Interval, Magnetic Resonance Imaging, Measurement

INTRODUCTION

Atlantooccipital dislocation is a serious injury and primarily an outcome of ligamentous disruption between the occiput and the upper cervical spine, often without accompanying bony fractures. This feature of these critical injuries renders this area likely to underestimate the injuries in this location.[1] Before interpreting the radiological images, one must be aware of specific details about the anatomical features of the craniocervical junction.

The biomechanical considerations and the risk of upper segment spinal injury made the researchers develop criteria in the assessment of the diagnostic approach for the radiology and instability of these injuries. Considering the spinal injury classifications, there are 2 important relationships in this region to consider for instability. These are atlantooccipital and atlantoaxial dislocations where clinicians and surgeons should indicate how to manage the proper approach to the patient. Powers ratio (PR), atlanto-dental interval (ADI), basion-dens interval (BDI), and basion-axial interval (BAI) come to the forefront to indicate these relationships in the literature.

Computerized tomography (CT) scan delineates the anatomic borders better by proper visualization of the bony cortex and this imaging technique is the modality of choice for craniocervical junction injuries.[2] On the other hand, magnetic resonance (MR) imaging reveals the integrity of the soft tissues, ligaments, and spinal cord better than CT. After the physical examination and the initial CT assessment, MR imaging is very useful to reveal any ligamentous or spinal injury after trauma, in clinically indicated patients. Even MR is considered in specific clinical situations, these intervals measured from specific landmarks of the craniocervical junction can also be observed in the field of view of MR images. The MR imaging assessment should be made in awareness of the craniocervical junction injuries and the critical intervals should also be measured during the interpretations where necessary to diagnose or consider an associated instability.

In this study, the researchers aimed to reveal the normative mean values of these critical intervals in patients without any cervical trauma, using MR images. The relationships between these intervals and age and any possible significant difference between genders were also attempted to be verified by proper statistical methods.

MATERIAL METHODS

Patients

This study was carried out in compliance with the basic principles outlined in the Declaration of Helsinki form (revised in 2013) and approved by the institutional ethics committee (Erzincan Binali Yıldırım University, Ethics Committee of Non-Interventional Research, Date: July 24, 2025- Numb: 464431). The requirement for the informed consent from each patient who participated in this study has been waived by the same ethics committee due to the retrospective nature of the study. The investigation was conducted as a retrospective, cross-sectional study and all patients who underwent lumbar MR imaging between June 1and June 30, 2025, were scanned. The study planned to find out the mean normative values of skeletally mature patients who had no cervical trauma; therefore, patients under 18 years old (n=7) and those with cervical trauma or fracture (n=23) were excluded. Considering the biomechanical alterations, 7 patients with scoliosis or kyphosis, 8 patients with spondylolisthesis, and 1 operated patient were excluded from the study. Hence, the lumbar MR images of 271 patients were included in the statistics without any possible biomechanical alterations that might influence the study results (Figure 1). All patients were measured by a radiology specialist with 8 years of experience, and the measurement results were recorded with 2 decimals after the comma. A picture archiving and communication system (Akgün PACS Viewer v7.5, Akgün Software, Ankara, Türkiye) was used to perform measurements on MR images in standard digital imaging communications in medicine formats.

Magnetic Resonance Imaging

All cervical MR images were acquired using a 1.5 tesla MR machine (Magnetom Aera, Siemens Healthcare, Erlangen, Germany). T1-weighted sagittal plane spin echo (TR [Time of repetition]: 663 ms, TE [Time of Echo]: 11 ms, FOV [Field of View]: 240 mm, Slice thickness: 3 mm, Voxel size: 0.9 × 0.9 × 3 mm; T2-weighted sagittal plane turbo spin echo (TR: 3800 ms, TE: 91 ms, FOV: 220 mm, Slice thickness: 3 mm, Voxel size: 0.7 × 0.7 × 3 mm) and T2-weighted axial plane turbo spin echo (TR: 780 ms, TE: 22 ms, FOV: 180 mm, Slice thickness: 3 mm, Voxel size: 0.4 × 0.4 × 3 mm) sequences were included in the imaging protocol. All patients were in a supine position, and all images were obtained using a neck coil with 20 channels.

Craniocervical Measurements

The T1-weighted midsagittal planes were used to measure PR, ADI, BDI, and BAI. To initiate, the interval between the basion point of the skull and the midpoint of the anterior cortex of the posterior arch of atlas (C1 vertebra) was measured. Then, the distance between the opistion point of the skull to the posterior cortex of the anterior arch of the atlas was indicated. The ratio of the first measured distance to the second interval has given the PR.[3] Atlanto-dental interval was measured as the line between the posterior edge of the anterior arch of atlas and the foremost part of the dens of axis. The distance between the most inferior edge of basion and the uppermost aspect of the dens axis was measured as BDI.[4] Basion-axial interval represented the distance between a line drawn tangentially to the posterior cortical surface of C2 and the basion[5] (Figure 2).

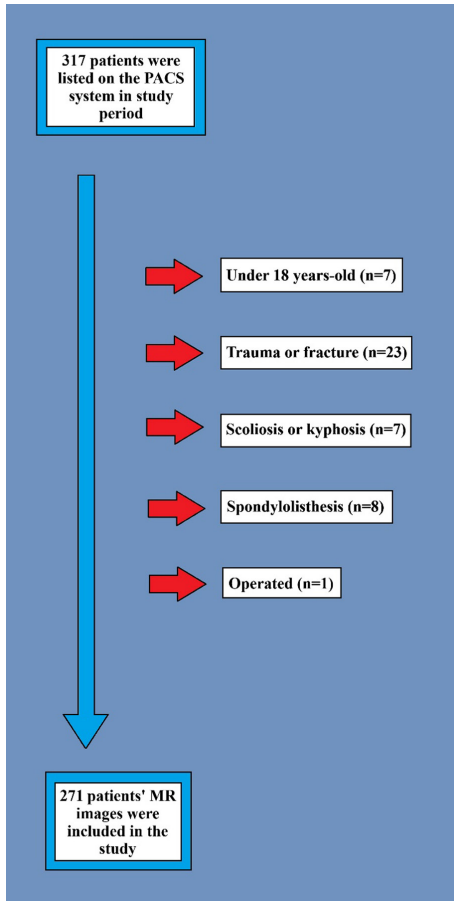

Figure 1. The workflow of the study (PACS: Picture Archiving and Communications System, MR: Magnetic Resonance).

Statistical Analysis

The statistical results of the study were performed by using IBM SPSS Statistics for Windows version 22.0 (IBM SPSS Corp.; Armonk, NY, USA). The Kolmogorov–Smirnov test was performed to determine the data distribution properties; additionally, boxplot graphics were used to represent the data distribution of the measurement results of each parameter for the total study population, females and males. The Mann–Whitney *U* tests were used to compare the results of female and male groups. The correlation between age and measurement results of each parameter, Spearman's Rho tests were carried out. The *P*-values of < .05 were considered to indicate statistical significance.

RESULTS

One hundred eighty-four females, 87 males, totally 271 patients' cervical MR images were re-assessed regarding PR, ADI, BDI, and BAI measurements. The mean age of the study population was 48.44 ±

MAIN POINTS

- This research was based on 4 critical craniocervical measurements and reveals the normative values using magnetic resonance images.
- The mean values of Powers ratio, atlanto-dental interval (ADI), basion-dens interval (BDI), and basion-axial interval were 0.76 ± 0.07, 1.14 ± 0.61 mm, 5.12 ± 1.74 mm, and 7.41 ± 2.20 mm, respectively, in this study.
- Males had higher ADI and BDI values than females according to the results of this investigation.
- Age showed a significant negative correlation regarding ADI and BDI measurements in this current research.

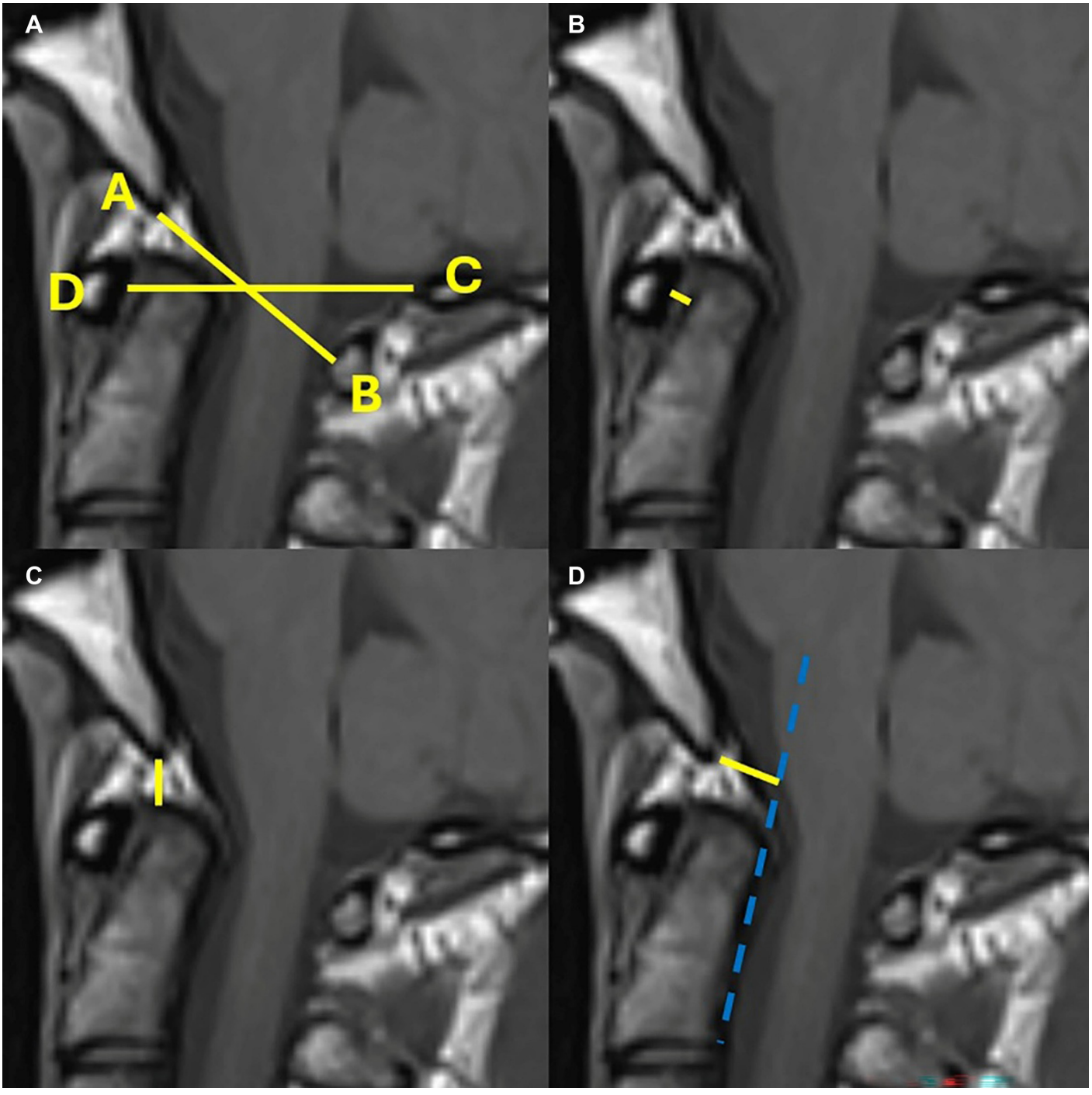

Figure 2. The distance between basion and the midpoint of the anterior cortex of the posterior arch of atlas is represented by the AB interval. The distance between the opistion to the posterior cortex of the anterior arch of the atlas is shown as the CD interval. The AB/CD ratio indicates the Powers ratio (A). The distance between the posterior edge of the anterior arch of atlas and the foremost part of the dens of axis is the atlanto-dental interval (B). The distance between the most inferior edge of basion and the uppermost aspect of the dens axis was measured as the basion-dens interval. A line drawn tangentially to the posterior cortical surface of C2 and the distance from basion to this line represented the basion-axial interval (D).

14.99. The female group was significantly older than the male group in the study population ($P = .002$) (Table 1).

The data distribution was analyzed by the Kolmogorov–Smirnov test and normal data distribution could not be reached regarding the ADI measurements. Hence, a non-parametric test (Mann–Whitney *U*) was considered to compare the results between the female and the male groups for ADI measurements. The data distribution results were shown by boxplot analyses (Figure 3).

Powers ratio and BAI indicated no significant difference between female and male groups. However, higher ADI ($P = .001$) and BDI

Table 1. Demographic Data of the Study Population

Gender (n)		Number		Percentage	
Females		184		67.9	
Males		87		32.1	
Total		271		–	
Age	**Mean**	**SD**	**Min**	**Max**	***P***
Females	50.31	15.19	18	84	**.002**
Males	44.47	13.83	18	76	
Total	48.44	14.99	18	84	–

The bold numbers indicate the significant difference.

(P = .017) values were obtained for males, compared with the female group (Table 2).

The correlation between age and PR, ADI, BDI, and BAI measurements was analyzed by Spearman's Rho tests. Age showed no significant correlation regarding PR and BAI measurements. There was a negative and moderate correlation between age and ADI, while BDI measurement results indicated a negative and very low correlation with age. According to the analyses with different gender groups, ADI revealed a negative moderate correlation for females and a negative low-level correlation for the male group regarding age (Table 3).

DISCUSSION

The study results of the current study indicated the mean values of PR, ADI, BDI, and BAI as 0.76 ± 0.07, 1.14 ± 0.61, 5.12 ± 1.74, and 7.41 ± 2.20 respectively. Female and male groups indicated a significant difference regarding ADI and BDI. Age showed a significant and negative correlation with ADI and BDI in the study population.

After the traumatic collisions or any suspicion of vertebral injuries to the head and neck region, CT is mostly considered in many health centers to investigate the abnormalities in the craniocervical junction. However, due to the superiority of MR imaging in the evaluation of the integrity of ligamentous structures in this specific location, this imaging modality is now more widely used than in the past. Before the interpretation of the cervical MR imaging, the doctors should know adequate information about patient history and be aware of the normal anatomic alignment of the osseous structures in this region. The normative values of the intervals between the critical anatomic reference points are a crucial part of the interpretation, along with the integrities of the bony and the ligamentous structures. Therefore one should be aware of the normative values of these critical intervals before the MR evaluations as well as for CT interpretations.

The upper segment cervical spinal injuries account for 56%-73% among all cervical traumas. Atlantooccipital dislocation is a serious injury associated with high mortality rates.[6] In postmortem studies, evidence of atlantooccipital dislocations has been reported in 20%-31% of deaths due to spinal injuries of the cervical region.[7] X-rays and CT scans are the most used imaging modalities for the initial screening of craniocervical junction traumas. The radiological criteria for craniocervical junction traumas have still been optimized. Harris et al's[8] method included BAI and BDI combined, was reported to be reliable in the guidelines published in 2013.[9] The PR was originally described to determine the anterior atlantooccipital injuries.[10] The normal value of the PR is less than 0.90, and this ratio is sensitive to distraction or posterior dislocation type atlantooccipital injuries.[1] On the other hand, an abnormally widened ADI is an indirect indicator of injury to the transverse atlantal ligament.[11]

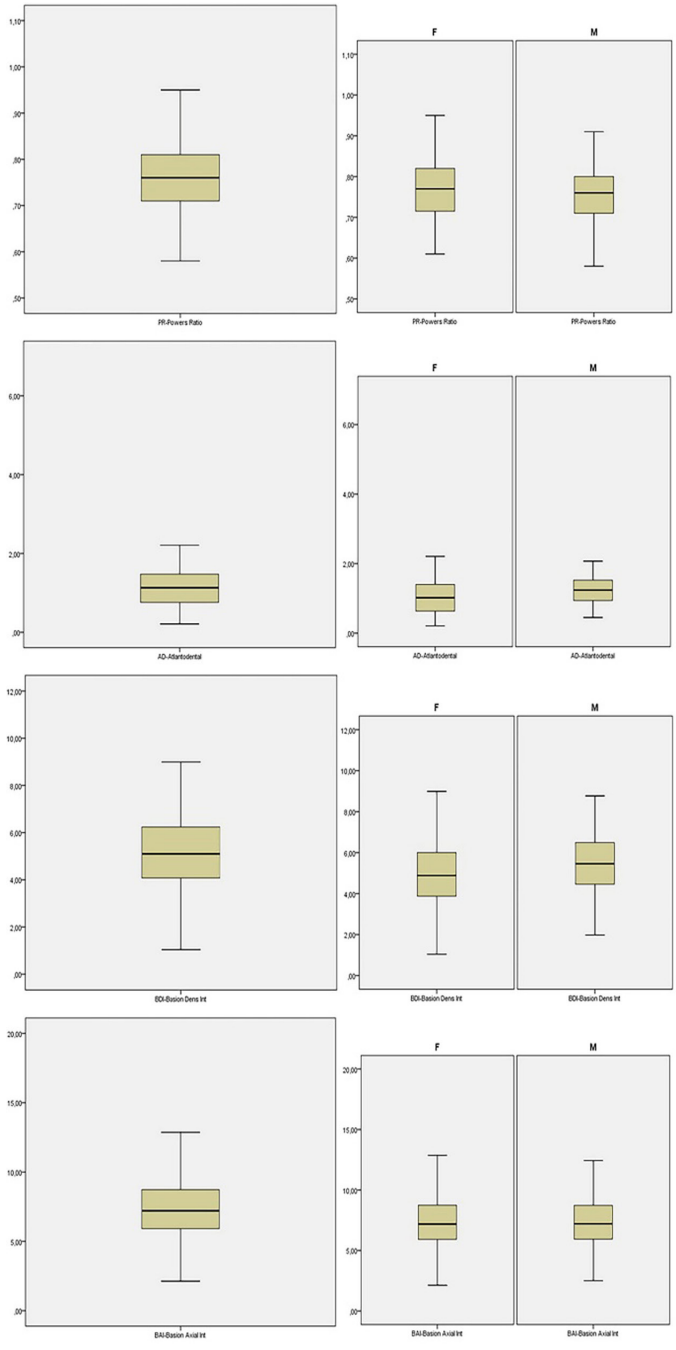

Figure 3. Boxplot graphics showing the data distribution for the total study population, females and males regarding the analysis of each parameter, Powers ratio, atlanto-dental interval (ADI), basion-dens interval (BDI), and BAI. Normal data distribution could not be reached regarding the ADI measurements (second row in the figure). Males had significantly higher ADI and BDI values than females in the study population of the research.

In a study by Martinez-del-Campo et al,[6] the patients with atlantooccipital dissociation (n=22) were compared with the control group (n=59) and performed the craniocervical measurements on CT images. The mean values of PR, BDI, and BAI were 0.71, 6.53, and 5.41, respectively, for the control group. Another study used CT images and was conducted on 200 patients examined for cervical spine injury, without osseous or soft tissue abnormality on initial CT

Table 2. The Comparison Between Females and Males Regarding Powers Ratio, Atlanto-Dental Interval, Basion-Dens Interval, and Basion-Axial Interval

	Mean	SD	*P*
PR			
Females	0.76	0.07	.397
Males	0.75	0.07	
Total	0.76	0.07	–
ADI (mm)			
Females	1.07	0.55	**.001**
Males	1.30	0.70	
Total	1.14	0.61	–
BDI (mm)			
Females	4.95	1.73	**.017**
Males	5.49	1.73	
Total	5.12	1.74	–
BAI (mm)			
Females	7.38	2.11	.794
Males	7.46	2.40	
Total	7.41	2.20	–

ADI, atlanto-dental interval; BAI, basion-axial intervals; BDI, basion-dens interval; mm, millimeter; PR, Powers ratio.

scan, and if the patients were discharged from the hospital without a diagnosis of a cervical spine injury. The mean values were 0.8, 1.3 mm, 5.7 mm, and 3.4 mm for PR, ADI, BDI, and BAI, respectively, in their study.[4] A cone-beam CT study indicated 0.72, 1.28 mm, 4.92 mm, and 4.01 mm mean values with regard to the measurements of PR, ADI, BDI, and BAI respectively.[12] Powers ratio, ADI, BDI, and BAI mean values were measured as 0.76, 1.14 mm, 5.12 mm, and 7.41, respectively.

The differences between the measured values in the current research might not be similar or close to some other researchers' studies, especially for the mean value of BAI measurement results. This might be a result of cortical irregularities regarding degenerative changes, and T1 weighted MR images might not reflect these alterations or delineate the cortical borders optimally and exaggerate the interval. On the other hand, these results may originate from the genetic differences between the study populations. Much more data obtained from the studies comparing the CT and MR results would be a lot better to verify this situation.

Table 3. The Correlation (Sperman's Rho) Analysis of Age and Powers Ratio, Atlanto-Dental Interval, Basion-Dens Interval, and Basion-Axial Interval for Total Study Population, Females and Males

		PR	ADI	BDI	BAI
Total (n = 271)					
Age	Correlation Coefficient	0.089	−0.480	−0.161	−0.075
	P	.145	**<.001**	**.008**	.216
Females (n = 184)					
Age	Correlation Coefficient	0.091	−0.531	−0.137	−0.049
	P	.221	**<.001**	.064	.511
Total (n = 87)					
Age	Correlation Coefficient	0.097	−0.233	−0.125	−0.184
	P	.370	**.030**	.248	.089

ADI, atlanto-dental interval; BAI, basion-axial interval; BDI, basion-dens interval; PR: Powers ratio,

This research was based on the 4 critical measurements to assess the craniocervical region, using MR images. Some important aspects should be considered before analyzing the results of this study. To begin with, many research results were discussed and compared with the current study results; however, some of these investigations were carried out with radiological modalities other than MR imaging. Additionally, the researchers performed measurements on T1-weighted sequences of MR imaging to depict the anatomical properties optimally. Computed tomography scan has the capacity to delineate the bony cortex and indicate the anatomical reference points better to measure the intervals. Even though the researchers aimed to underline the awareness of the morphological outcomes of the craniocervical trauma during MR image interpretations, the intervals can be measured on CT images more accurately. The data distributions of this research indicated a significant age difference between the female and the male group. Moreover, ADI results should also be discussed carefully since normal data distribution could not be reached due to the measurement results. Because of the data properties in the study population, these conditions should also be accepted as additional limitations before interpreting the results of the study.

In conclusion, MR imaging is a significant method to assess the ligamentous and spinal parameters of cervical trauma; however, to understand the secondary signal alterations of the traumatic impact one should be aware of the critical intervals to evaluate the craniocervical region better in MR image interpretations. Simple but useful parameters, which were important to make critical decisions, were measured on MR images, and the measurement results were discussed with the ranges in CT examinations to establish the normative values of MR imaging. Further studies are needed to verify these results, and these mean values and the influence of age and gender on these parameters should also be compared with the measurement results of larger series from different populations.

Data Availability Statement: The data that support the findings of this study are available on reasonable request from the corresponding author.

Ethics Committee Approval: This study is approved by the institutional ethics committee of Erzincan Binali Yıldırım University Ethics Committee of Non-Interventional Research, Date: July 24, 2025- Number: 469488).

Informed Consent: The requirement for the informed consent from each patient participating in this study has been waived by the ethics committee regarding the methodology of the research.

Peer-review: Externally peer-reviewed.

Author Contributions: Concept – B.K.; Design – B.K.; Resources – F.Ö.; Materials – F.Ö.; Data Collection and/or Processing – B.K, F.Ö.; Analysis and/or Interpretation – B.K, F.Ö.; Literature Search – F.Ö.; Writing Manuscript – B.K.; Critical Review – F.Ö.

Declaration of Interests: The authors have no conflict of interest to declare.

Funding: The authors declared that this study has received no financial support.

REFERENCES

1. Hall GC, Kinsman MJ, Nazar RG, et al. Atlanto-occipital dislocation. *World J Orthop*. 2015;6(2):236-243. [CrossRef]
2. Siddiqui J, Grover PJ, Makalanda HL, Campion T, Bull J, Adams A. The spectrum of traumatic injuries at the craniocervical junction: a review of

imaging findings and management. *Emerg Radiol*. 2017;24(4):377-385. [CrossRef]
3. Baker JF. Analysis of upper cervical spine measurements in the uninjured pediatric spine. *Int J Spine Surg*. 2022;16(3):458-464. [CrossRef]
4. Rojas CA, Bertozzi JC, Martinez CR, Whitlow J. Reassessment of the craniocervical junction: normal values on CT. *AJNR Am J Neuroradiol*. 2007;28(9):1819-1823. [CrossRef]
5. Akpolat AO, Kilinc BE, Aksay MF, Balioglu MB. Is it necessary to evaluate the craniocervical junction with computed Tomoghraphy in adolescent spinal deformities? *Turk Neurosurg*. 2021;31(3):441-446. [CrossRef]
6. Martinez-Del-Campo E, Kalb S, Soriano-Baron H, et al. Computed tomography parameters for atlantooccipital dislocation in adult patients: the occipital condyle-C1 interval. *J Neurosurg Spine*. 2016;24(4):535-545. [CrossRef]
7. Ehlinger M, Charles YP, Adam P, et al. Survivor of a traumatic atlanto-occipital dislocation. *Orthop Traumatol Surg Res*. 2011;97(3):335-340. [CrossRef]
8. Harris JH Jr, Carson GC, Wagner LK. Radiologic diagnosis of traumatic occipitovertebral dissociation: 1. Normal occipitovertebral relationships on lateral radiographs of supine subjects. *AJR Am J Roentgenol*. 1994;162(4):881-886. [CrossRef]
9. Theodore N, Aarabi B, Dhall SS, et al. The diagnosis and management of traumatic atlanto-occipital dislocation injuries. *Neurosurgery*. 2013;72(Suppl 2):114-126. [CrossRef]
10. Powers B, Miller MD, Kramer RS, Martinez S, Gehweiler JA. Traumatic anterior atlanto-occipital dislocation. *Neurosurgery*. 1979;4(1):12-17. [CrossRef]
11. Deliganis AV, Baxter AB, Hanson JA, et al. Radiologic spectrum of craniocervical distraction injuries. *RadioGraphics*. 2000;20(special No.):S237-S250. [CrossRef]. Erratum in: *RadioGraphics*. 2001;21(2):520.
12. Tanrisever S, Orhan M, Bahşi İ, Yalçin ED. Anatomical evaluation of the craniovertebral junction on cone-beam computed tomography images. *Surg Radiol Anat*. 2020;42(7):797-815. [CrossRef]

Current Research in MRI

Original Article

Cut-Off Point Values for the Number and Average Size of T2 Hyperintense Focies in the Brain White Matter

Lala Guluzade[1], Malakhat Sultanova[2], Hasan Isayev[1]

[1]Department of Radiology, Zafaran Hospital, Baku, Azerbaijan
[2]Department of Radiology, Azerbaijan Medical University, Baku, Azerbaijan

Cite this article as: Guluzade L, Sultanova M, Isayev H. Cut-off point values for the number and average size of T2 hyperintense focies in the brain white matter. *Current Research in MRI*, 2025;4(2):45-49.

Corresponding author: Lala Guluzade, e-mail: dr.guluzade@gmail.com

Received: September 7, 2025 **Accepted:** October 8, 2025 **Publication Date:** October 30, 2025

DOI: 10.5152/CurrResMRI.2025.25132

Abstract

Objective: The aim of this study is to determine the cut-off values for the increase in the number and average size of T2 hyperintense focies in the brain white matter in patients with arterial hypertension (AH), type 2 diabetes mellitus (T2DM), both conditions combined, and in healthy individuals.

Methods: A total of 275 patients aged between 35 and 70 years were included in the study. The imaging was performed using a Siemens Magnetom Aera 1.5 Tesla magnetic resonance imaging device. T2 hyperintense foci were assessed using the turbo inversion recovery magnitude sequence with a slice thickness of 3.5 mm and a 10% interslice gap. Quantitative and qualitative data obtained during the study were analyzed using variation, discriminant, dispersion, correlation, Receiver Operating Characteristic (ROC) analysis, and evidence-based medicine methods with MS Excel 2019 and IBM SPSS Statistics 26 software.

Results: In healthy individuals, the cut-off point for the number of focies was determined to be 12, and the average focus size was 2.9 mm. In patients with AH, the cut-off value was 14 foci with a mean size of 1.9 mm. For those with T2DM, the corresponding values were 14 foci and 2.9 mm in average size. In individuals with both AH and T2DM, the cut-off point was 23 for foci, while the average foci size was 2.9 mm.

Conclusion: By establishing group-specific cut-off values, this study provides clinicians with a useful reference point to support differential diagnosis in routine practice.

Keywords: Cut-off point, hypertension, magnetic resonance tomography (MRT), T2 hyperintense foci, type 2 diabetes mellitus

INTRODUCTION

Strong clinical evidence from tomographic and physical examinations indicates that white matter hyperintensities increase the risk of stroke, cognitive decline, mortality, depression, gait disturbances, and motor dysfunctions.[1,2] These foci are associated with brain atrophy, complications of small vessel disease, focal progressive brain damage, and underlying silent brain injuries, which contribute to infarct expansion and deterioration of major arterial stroke regions. They serve as neuroradiological markers of brain impairment.[3]

Age-related enlargement of perivascular spaces, increased interstitial fluid concentration, heightened blood-brain barrier permeability, and plasma pooling result in combined foci with periventricular localization observable on magnetic resonance imaging (MRI) scans. Histopathologically, these areas correspond to mild demyelination.[4,5] However, since autopsy is inaccessible for living patients, it is crucial to differentiate these foci using diagnostic MRI. Literature reports that T2 hyperintense foci are more frequently observed in elderly patients, although not all of them demonstrate histopathological demyelination.[4,6] Nevertheless, in contemporary practice, it remains challenging to distinguish which portion of these foci in older adults is related to aging and which is associated with underlying diseases. Recent studies employing functional MRI have examined that even in healthy adults, the localization of T2 hyperintense foci may contribute to specific cognitive impairments.[7]

Researchers have emphasized that in migraine patients, the presence of aura and the severity of headaches increase the number of T2 hyperintense foci; however, the specific brain regions where these foci predominantly develop remain under investigation.[8]

Additionally, the relationship between T2 hyperintense foci and gender has been studied, revealing a slightly higher prevalence in females. Nevertheless, over 80% of the variance in these gender differences remains unexplained. The study of T2 hyperintense foci in white matter should advance beyond cerebrovascular diseases to broader neurological contexts.[9]

Furthermore, investigators have explored the association between diabetes mellitus and T2 hyperintense focies.[10,11] Notably, type 2 diabetes mellitus is linked with an increased number of these foci. The localization of T2 hyperintense foci in periventricular and deep white matter reflects their differing pathological characteristics. Clinically, periventricular foci are associated with brain atrophy, while deep white matter foci correlate with cerebrovascular events.

Considering the issues highlighted above, it was deemed essential to investigate clinically relevant problems that will enhance the diagnostic accuracy of T2 hyperintense focies.

MATERIAL AND METHODS

The study included MRI results of the brain conducted between 2020 and 2023 from 275 patients in ..... Hospital and ..... University. The control group consisted of 86 healthy individuals, and results were compared across all groups. Among the patients, 77 had arterial hypertension (AH), 51 had type 2 diabetes mellitus (T2DM), and 61 had both AH and T2DM. This is a non-invasive method; that is why there is no informed consent. Ethics committee of University of Azerbaijan Medical University (Approval No 22, Date 09.07.2022). The age range of the participants was between 35 and 70 years. To exclude age-related T2 hyperintense foci associated with advanced aging, patients over 70 years old were not included in the study. Individuals with a history of oncological diseases, brain trauma, brain surgery, demyelinating disorders, granulomatous diseases, alcohol abuse, or diagnosed with migraine were excluded from the research. Due to these factors, the presence of white matter hyperintensities formed by such causes could potentially lead to inaccurate results in the study. Patients with AH included in the research had elevated systolic blood pressure ranging from 140 to 200 mmHg. The duration of disease in AH patients ranged from 10 to 15 years, while in patients with T2DM, it ranged between 5 and 10 years. Only patients diagnosed with T2DM who had blood glucose levels above 7 mmol/L were included. Patients selected for this study were those referred to the clinic for brain MRI examinations due to various complaints such as headache, dizziness, head pressure, nausea, hemiparesis-hemiplegia, gait and behavioral disturbances, facial drooping, facial numbness, among others.

This study utilized high-resolution T2 turbo inversion recovery magnitude (TIRM) images acquired using a 1.5 Tesla Siemens Magnetom Aera MRI scanner. During the brain MRI examinations, all patients underwent imaging in the following sequences: axial, coronal, and sagittal T2; axial TIRM; sagittal isometric T1; and susceptibility-weighted imaging, which is more sensitive to hemosiderin and calcium deposits. For this study, the axial TIRM sequence was specifically employed. The T2 TIRM images were obtained with parameters TR = 9200 ms, TI = 2450 ms, TE = 84 ms, slice thickness of 3.5 mm, and an interslice gap of 10% of the slice thickness.

Regarding the study design, it is classified as analytical; by methodology, clinical; by scale, selective; by type, scientific; by material, prospective; by duration, cross-sectional; and by location, clinical.

MAIN POINTS

- Arterial hypertension (AH), type 2 diabetes mellitus, and their combination significantly influence the increase in both the number and size of T2 hyperintense focies detected during brain magnetic resonance imaging (MRI) examinations.
- The cut-off values for the number and average size of T2 hyperintense foci identified by brain MRI in patients without a history of AH or type 2 diabetes can serve as predictive markers for these conditions.
- There is a statistically significant positive correlation between the number and average size of T2 hyperintense foci in patients with AH, type 2 diabetes mellitus, or both. As the number of foci increases, their size also grows, indicating greater damage to the brain parenchyma.

Quantitative and qualitative data collected during the study were analyzed using variation, discriminant, dispersion, correlation, ROC analysis, and evidence-based medicine methods via MS Excel 2019 and IBM SPSS Statistics 26 (IBM SPSS Corp.; Armonk, NY, USA) software.

Quantitative data are expressed in tables as mean ± standard error (M, ±m) and median with interquartile ranges (Me, Q1, Q3). For group comparisons, the Mann–Whitney *U*-test, Student's *t*-test with Bonferroni correction, and Kruskal-Wallis tests were applied.

ROC analysis was performed using a binary classification model, constructing the integral value of sensitivity and specificity (ROC curve) across the entire range of the studied parameters. The area under the ROC curve was calculated and statistically evaluated. Identification of cut-off points, which represent the farthest point from the reference line on the ROC curve, allows the test to be used as a selection criterion in future studies.[12]

RESULTS

T2 hyperintense foci were detected in 51 patients in the control group, 68 patients with AH, 46 patients with T2DM, and 56 patients with both AH and T2DM. The presence of AH, T2DM, and their combination significantly increased both the number and size of T2 hyperintense focies in the brain compared to the control group ($p_F < 0.001$, $p_H < 0.001$) (Graph 1).

As shown in the Graph 2 below, the area under the ROC curve representing the integral sensitivity and specificity for the number of foci in the practically healthy control group was 0.862 ± 0.023. For the average foci size, it was 0.758 ± 0.033. Comparison between the control group and all other groups demonstrated statistically significant lower foci numbers and sizes in the control group ($P < .001$).

The cut-off point for the number of foci in the healthy control group was established at 12 (sensitivity 71.6 ± 3.0%, specificity 94.1 ± 3.3%, accuracy 75.8 ± 2.6%). For the average foci size, the cut-off was 2.9 mm (sensitivity 47.3 ± 3.4%, specificity 92.2 ± 3.8%, accuracy 55.7 ± 3.0%).

Therefore, having fewer than 12 foci and an average foci size smaller than 2.9 mm serves as an informative indicator for identifying healthy individuals.

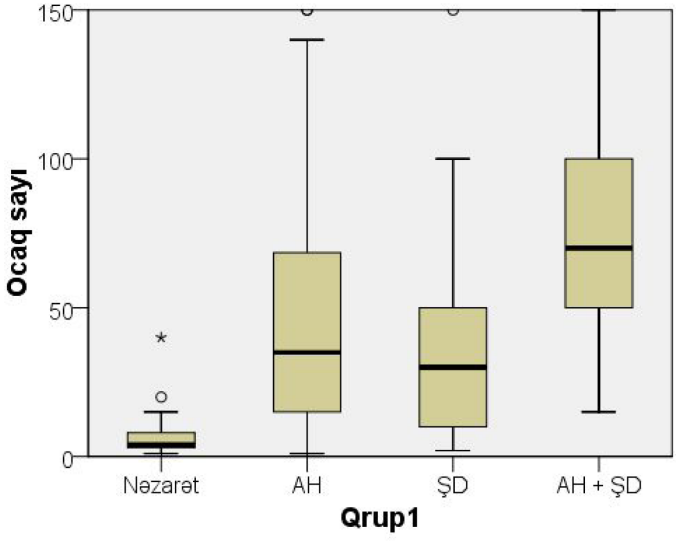

Graph 1. Comparative evaluation number of foci among main gGroups.

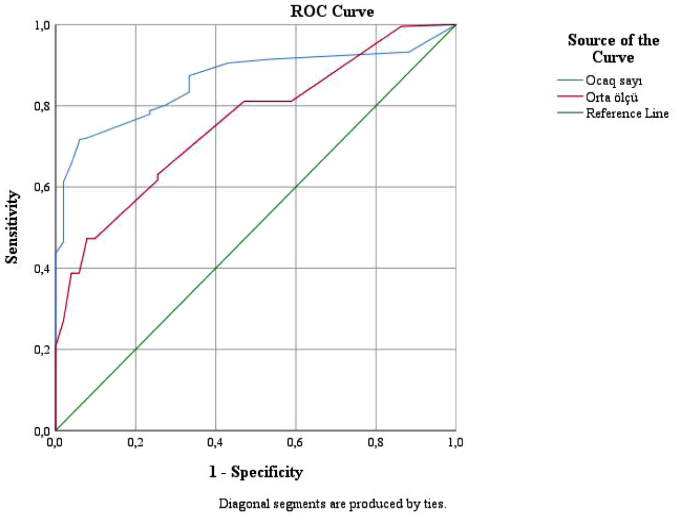

Graph 2. Area under the ROC curve for foci number and average size in the control group.

Test Result Variable(s)	Area	Std. Error	Asymptotic Sig.	Asymptotic 95% CI Lower Bound	Asymptotic 95% CI Upper Bound
Number of foci	0.862	0.023	0.000	0.817	0.906
Average size	0.758	0.033	0.000	0.693	0.822

As illustrated in the Graph 3 below, the area under the ROC curve representing the combined sensitivity and specificity for the diagnosis of AH is 0.901 ± 0.029. For the average foci size, this value is 0.760 ± 0.043.

The cut-off point for the number of foci in patients with AH is 14 (sensitivity 77.9 ± 5.0%, specificity 94.1 ± 3.3%, accuracy 84.9 ± 3.3%). For the average foci size, the cut-off is 1.9 mm (sensitivity 83.8 ± 4.5%, specificity 52.9 ± 7.0%, accuracy 70.6 ± 4.2%).

Thus, having more than 14 foci and an average foci size greater than 1.9 mm serves as an informative marker for the presence of AH.

Test Result Variable(s)	Area	Std. Error	Asymptotic Sig.	Asymptotic 95% CI Lower Bound	Asymptotic 95% CI Upper Bound
Number of foci	0.901	0.029	0.000	0.843	0.959
Average size	0.760	0.043	0.000	0.676	0.845

In patients with T2DM, the cut-off point for the number of focies was determined to be 14. Thus, having more than 14 foci serves as an informative indicator for the presence of T2DM. Among 46 T2DM patients, 33 had foci counts exceeding this threshold. For this cut-off value, sensitivity was calculated as 71.7 ± 6.6%. Among 51 practically healthy individuals, 48 had fewer than 14 foci, resulting in a specificity of 94.1 ± 3.3%. The overall diagnostic accuracy of the test was 83.5 ± 3.8%.

The positive predictive value (PPV) for detecting more than 14 foci was 91.7 ± 4.6%, while the negative predictive value (NPV) was 78.7 ± 5.2%.

In patients with T2DM, the cut-off point for the average foci size was determined to be 2.9 mm. Thus, an average foci size greater than 2.9 mm serves as an informative indicator for the presence of T2DM. Among the 46 patients with T2DM, 21 had an average foci size exceeding this threshold. For this cut-off point, sensitivity was calculated as 45.7 ± 7.3%. Among 51 healthy individuals, 47 had average foci sizes smaller than 2.9 mm, yielding a specificity of 92.2 ± 3.8%. The overall diagnostic accuracy of the test was 70.1 ± 4.6%. The PPV for identifying average foci sizes greater than 2.9 mm was 84.0 ± 7.3%, and the NPV was 65.3 ± 5.6%.

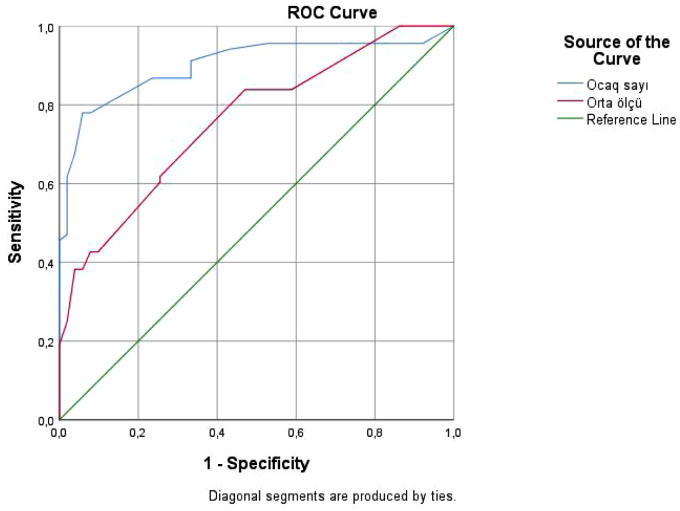

Graph 3. Area under the ROC curve for foci number and average size in the arterial hypertension group.

In patients with both AH and T2DM, the cut-off point for the number of focies was determined to be 23. Thus, having more than 23 foci serves as an informative marker for the presence of concurrent AH and T2DM. Among the 56 patients with AH+T2DM, 54 had foci counts exceeding this threshold. For this cut-off value, sensitivity was calculated as 96.4 ± 2.5%. Among 51 healthy individuals, 47 had fewer than 23 foci, resulting in a specificity of 98.0 ± 1.9%. The overall diagnostic accuracy of the test was 97.2 ± 1.6%.

The PPV for foci counts greater than 23 was 98.2 ± 1.8%, while the NPV was 96.2 ± 2.7%.

In patients with both AH and T2DM, the cut-off point for the average foci size was identified as 2.9 mm. Thus, an average foci size greater than 2.9 mm serves as an informative indicator for the presence of AH+T2DM. Among the 56 patients with AH+T2DM, 41 had average foci sizes exceeding this threshold. For this cut-off value, the sensitivity was 73.2 ± 5.9%. Among 51 practically healthy individuals, 47 had average foci sizes smaller than 2.9 mm, yielding a specificity of 92.2 ± 3.8%. The overall diagnostic accuracy of the test was 82.2 ± 3.7%.

The PPV for average foci sizes greater than 2.9 mm was 91.1 ± 4.2%, while the NPV was 75.8 ± 5.4%.

DISCUSSION

T2 hyperintense focies—particularly those with a tendency to merge—have been shown to impair cognitive functions such as memory, executive functioning, and response speed.[13] In light of such findings, investigating the underlying causes of T2 hyperintense foci is of great

importance in order to implement preventive measures. Magnetic resonance imaging remains the most suitable non-invasive method for detecting T2 hyperintense foci, and it also allows for follow-up imaging to monitor changes over time.

Not only the number, but also the progression rate of these foci has been associated with the development of dementia.[14] Larger foci, especially those prone to confluence, may lead to disability within 1 year.[14] This study similarly found that as the number of foci increased, their average size also grew, resulting in more extensive damage to the brain parenchyma. This supports the hypothesis that a higher foci number increases the likelihood of foci merging. This finding demonstrated a statistically significant positive correlation ($P < .001$).

T2 hyperintense foci can be evaluated using visual-manual assessment, as well as semi-automated or fully automated methods. However, automated techniques are often costly.[14] Therefore, the visual-manual method remains practical and accessible for most clinical settings. The findings obtained in this study can be effectively utilized by radiologists in routine diagnostic practice.

Alzheimer's disease manifests with dementia symptoms in 40%-80% of cases, with vascular factors cited as the primary etiology. T2 hyperintense focies detected on brain MRI serve as independent risk factors for dementia and cognitive decline, even in the absence of concurrent brain injury.[15]

There is strong evidence that hypertension independently contributes to the development and progression of T2 hyperintense foci. Studies indicate that individuals with hypertension and a high burden of T2 hyperintense foci exhibit these foci predominantly in areas of cerebral hypoperfusion. Hypertension leads to microstructural white matter damage that persists despite adequate treatment.[16] Preventing or treating hypertension is therefore a vital step in slowing the progression of T2 hyperintense foci and preserving brain health with advancing age. The presence of T2 hyperintense foci doubles the risk of dementia and triples the risk of stroke.[16]

The number of patients with T2DM continues to rise, posing a significant global health concern. The likelihood of microvascular complications is closely linked to T2DM. There is substantial evidence that T2DM causes structural brain anomalies such as T2 hyperintense foci, lacunar infarcts, and brain atrophy. Sun et al[17] investigated these changes in their compatriots, the Chinese population. T2 hyperintense foci represent silent brain injuries located in the periventricular and deep white matter. Although hypertension is a risk factor for T2 hyperintense foci, studies indicate that diabetes contributes to the formation of more numerous and larger T2 hyperintense focies.[17]

Over the past decades, both AH and T2DM have reached epidemic proportions.[18] When coexisting, T2DM and AH exhibit a synergistic effect, increasing the risk of both microvascular and macrovascular complications.[19,20] According to global assessments, over 50% of individuals with diabetes are diagnosed with AH. Epidemiological data show that the risk of dementia in diabetic patients without hypertension is 19%, whereas this risk rises to 23% in patients with both diabetes and hypertension.[21,22]

Globally, approximately 45.8% of adults with diabetes remain undiagnosed, which leads to untreated conditions and increased risk of complications.[23,24] According to the World Health Organization, about half (46%) of patients with AH are unaware of their condition.[25]

During this study, several limitations were noted. Firstly, the authors were unable to evaluate and compare the findings using fully automated systems. Secondly, they did not establish a direct clinical correlation between the detected foci and dementia.

In conclusion, based on the values obtained (along with appropriate specificity and sensitivity percentages), a subset of patients with detected T2 hyperintense foci are considered as healthy without suspected pathology. Additionally, in patients unaware of their AH or T2DM, the number and size of T2 hyperintense focies detected during brain MRI—performed due to headaches or other reasons—can guide radiologists in advising treating physicians and clinicians by utilizing the identified cut-off point values. Therefore, these findings are regarded as highly valuable.

Data Availability Statement: The data that support the findings of this study are available on request from the corresponding author.

Ethics Committee Approval: Ethical committee approval was received from the Ethics committee of University of Azerbaijan Medical University (Approval No 22, Date 09.07.2022).

Informed Consent: Informed consent was not obtained from the patients as the study method is non-invasive.

Peer-review: Externally peer-reviewed.

Author Contributions: Concept – M.S.; Design – H.I.; Supervision – M.S.; Resources – L.G.; Materials – L.G.; Data Collection and/or Processing – L.G.; Analysis and/or Interpretation – M.S.; Literature Search – L.G.; Writing Manuscript – L.G.; Critical Review – M.S.

Declaration of Interests: The authors have no conflict of interest to declare.

Funding: The authors declared that this study has received no financial support.

REFERENCES

1. Altermatt A, Gaetano L, Magon S, et al. Clinical associations of T2-weighted lesion load and lesion location in small vessel disease: insights from a large prospective cohort study. *Neuroimage*. 2019;189:727-733. [CrossRef]
2. Amier RP, Marcks N, Hooghiemstra AM, et al. Hypertensive exposure markers by MRI in relation to cerebral small vessel disease and cognitive impairment. *JACC Cardiovasc Imaging*. 2021;14(1):176-185. [CrossRef]
3. Wardlaw JM, Chappell FM, Valdés Hernández MDC, et al. White matter hyperintensity reduction and outcomes after minor stroke. *Neurology*. 2017;89(10):1003-1010. [CrossRef]
4. Haller S, Kövari E, Herrmann FR, et al. Do brain T2/FLAIR white matter hyperintensities correspond to myelin loss in normal aging? A radiologic-neuropathologic correlation study. *Acta Neuropathol Commun*. 2013;1:14. [CrossRef]
5. Han F, Zhai FF, Wang Q, et al. Prevalence and risk factors of cerebral small vessel disease in a Chinese population-based sample. *J Stroke*. 2018;20(2):239-246. [CrossRef]
6. Hughes D, Judge C, Murphy R, et al. Association of blood pressure lowering with incident dementia or cognitive impairment: a systematic review and meta-analysis. *JAMA*. 2020;323(19):1934-1944. [CrossRef]
7. Lampe L, Kharabian-Masouleh S, Kynast J, et al. Lesion location matters: the relationships between white matter hyperintensities on cognition in the healthy elderly. *J Cereb Blood Flow Metab*. 2019;39(1):36-43. [CrossRef]
8. Negm M, Housseini AM, Abdelfatah M, Asran A. Relation between migraine pattern and white matter hyperintensities in brain magnetic resonance imaging. *Egypt J Neurol Psychiatr Neurosurg*. 2018;54(1):24. [CrossRef]

9. Sachdev PS, Parslow R, Wen W, Anstey KJ, Easteal S. Sex differences in the causes and consequences of white matter hyperintensities. *Neurobiol Aging*. 2009;30(6):946-956. [CrossRef]
10. Tamura Y, Kimbara Y, Yamaoka T, et al. White matter hyperintensity in elderly patients with diabetes mellitus is associated with cognitive impairment, functional disability, and a high glycoalbumin/glycohemoglobin ratio. *Front Aging Neurosci*. 2017;9:220. [CrossRef]
11. Tchistiakova E, Anderson ND, Greenwood CE, MacIntosh BJ. Combined effects of type 2 diabetes and hypertension associated with cortical thinning and impaired cerebrovascular reactivity relative to hypertension alone in older adults. *NeuroImage Clin*. 2014;5:36-41. [CrossRef]
12. Qafarov İA. *Biostatistika*. Baku, Azerbaijan: 2021, 238 s
13. Wang L, Goldstein FC, Levey AI, et al. White matter hyperintensities and changes in white matter integrity in patients with Alzheimer's disease. *Neuroradiology*. 2011;53(5):373-381. [CrossRef]
14. Gorelick PB, Scuteri A, Black SE, et al. Vascular contributions to cognitive impairment and dementia: a statement for healthcare professionals from the American Heart Association/American Stroke Association. *Stroke*. 2011;42(9):2672-2713. [CrossRef]
15. SPRINT MIND Investigators for the SPRINT Research Group, Nasrallah IM, Pajewski NM, Auchus AP, et al. Association of intensive vs standard blood pressure control with cerebral white matter lesions. *JAMA*. 2019;322(6):524-534. [CrossRef]
16. Zhao Y, Ke Z, He W, Cai Z. Volume of white matter hyperintensities increases with blood pressure in patients with hypertension. *J Int Med Res*. 2019;47(8):3681-3689. [CrossRef]
17. Sun J, Xu B, Zhang X, et al. The mechanisms of type 2 diabetes-related white matter intensities: a review. *Front Public Health*. 2020;8:498056. [CrossRef]
18. Yang C, DeVisser A, Martinez JA, et al. Differential impact of diabetes and hypertension in the brain: adverse effects in white matter. 2011;42(3):446-458. *Neurobiol Dis*. [CrossRef]. Retraction in: *Neurobiol Dis*. 2014;68:228. 10.1016/j.nbd.2014.05.005
19. de Havenon A, Majersik JJ, Tirschwell DL, McNally JS, Stoddard G, Rost NS. Blood pressure, glycemic control, and white matter hyperintensity progression in type 2 diabetics. *Neurology*. 2019;92(11):e1168-e1175. [CrossRef]
20. Dufouil C, Chalmers J, Coskun O, et al. Effects of blood pressure lowering on cerebral white matter hyperintensities in patients with stroke: the PROGRESS (perindopril Protection Against Recurrent Stroke Study) magnetic resonance imaging Substudy. *Circulation*. 2005;112(11):1644-1650. [CrossRef]
21. Newby D, Garfield V. Understanding the inter-relationships of type 2 diabetes and hypertension with brain and cognitive health: a UK Biobank study. *Diabetes Obes Metab*. 2022;24(5):938-947. [CrossRef]. Erratum in: *Diabetes Obes Metab*. 2022;24(12):2482. 10.1111/dom.14848
22. No HJ, Yi HA, Won KS, Chang HW, Kim HW. Association between white matter lesions and the cerebral glucose metabolism in patients with cognitive impairment. *Rev Esp Med Nucl Imagen Mol (Engl Ed)*. 2019;38(3):160-166. [CrossRef]
23. Zheng Y, Ley SH, Hu FB. Global aetiology and epidemiology of type 2 diabetes mellitus and its complications. *Nat Rev Endocrinol*. 2018;14(2):88-98. [CrossRef]
24. Zhuo Y, Fang F, Lu L, et al. White matter impairment in type 2 diabetes mellitus with and without microvascular disease. *NeuroImage Clin*. 2019;24:101945. [CrossRef]
25. World health organization. [Electronic resource] / - August 25, 2021. Available at: https://www.who.int/news-room/fact-sheets/detail/hypertension.